12-2021

Investigation of N-sulfonyliminium Ion Triggered Cyclizations for the Synthesis of Piperidine Scaffolds

Kaitlyn Birkhoff

Investigation of N-sulfonyliminium Ion Triggered Cyclizations for the Synthesis of Piperidine Scaffolds

by

Kaitlyn Marie Birkhoff

A Thesis
Submitted to the Honors College of
The University of Southern Mississippi
in Partial Fulfillment
of Honors Requirements

December 2021

Approved by:

Matthew Donahue, Ph.D., Thesis Advisor,
School of Mathematics and Natural Sciences

Bernd Schroeder, Ph.D., Director,
School of Mathematics and Natural Sciences

Sabine Heinhorst, Ph.D., Dean
Honors College

ABSTRACT

In consideration of the on-going global pandemic, immediate access to Food and Drug Administration approved pharmaceutical medications and vaccines is a matter of utmost priority to our national healthcare system. One significant modality in managed care is the dispensation of prescription drugs for the prevention or treatment of illnesses and diseases. According to the Centers for Disease Control and Prevention, physicians order and provide over 2.9 billion prescriptions each year with analgesics, antihyperlipidemics, and dermatological agents being the most prescribed therapeutic classes. Within those classes exists a disparate variety of chemical structures that must be prepared on a metric ton scale to meet the continual societal demand.

The piperidine scaffold is very prevalent in many FDA approved drugs, making it an important pharmacophore and essential in the field of drug discovery. Piperidines are the building blocks for over 70 different types of commercial drugs, such as Ritalin and Evista. The complexity of these structures along with the economic costs of sourcing all the raw materials is a contributing factor to the increasing burden of prescription drug costs. Therefore, by developing new chemical reactions to access the piperidine scaffold, the economic and chemical challenges can be effectively managed to ensure healthcare demands are met. The overarching goal of this project is to develop a robust catalytic, asymmetric synthesis of piperidine rings from feedstock petrochemicals.

In an initial study of the N-sulfonyl iminium ion Pictet-Spengler cyclization with N-para-toluenesulfonyl homoveratrylamine and 3-phenylpropanal, a screen of metal triflates was examined. The hypothesis is that transition metal triflates are sufficiently Lewis acidic to activate relatively inert sulfonamide nitrogen atoms to condense with

aldehydes and trigger the intramolecular cyclization forming piperidines. Initial results indicated that scandium (III), stannous (II) and copper (II) triflates gave the fastest conversion to the N-sulfonyl piperidine, while triflates such as lanthanum (III), sodium (I) and magnesium (II) gave little to no conversion under the allotted time. Further examinations were made to study the steric effects of the aldehyde carbon chain and hybridization, as well as the N-sulfonyl group substituent on cyclization conversion. A second acid catalyst screen was conducted of the N-sulfonyl iminium ion Aza Prins/Ritter reaction with N-sulfonyl homoallylic amine and 3-phenylpropanal to observe the difference between Bronsted acids and Lewis acids on cyclization conversion.

The fundamental investigation of chemical reactivity for the synthesis of nitrogen heterocycles from petroleum feedstocks has significant impact on societal healthcare needs. The control of reaction variables such as catalyst and ligand architectures in asymmetric transformations increases our understanding of interactions at the atomic level. Additional studies have focused on the use of chiral ligands, such as PyBOX ligands to induce asymmetry in the cyclization event. When screened against N-para-toluenesulfoyl homoveratrylamine with the successful metal triflates (scandium (III) and copper (II)) under various solvents, preliminary results showed no conversion towards the piperidine product. Future studies will focus on examining the kinetics of chiral ligand mechanisms and increasing the reactivity of iminium ions.

Keywords: piperidine, Pictet-Spengler, pharmacaphore, transition-metal triflates, asymmetric catalysis, enantioselectivity

DEDICATION

This honors thesis is dedicated to my family, friends, colleagues, and mentors, who have supported me over the past 4 years. I would like to specifically dedicate this thesis to my parents for their unwavering support and confidence in me throughout my college experience, as well as my lab mates for being a second family and a home-away-from home.

ACKNOWLEDGMENTS

I would like to thank my advisor, Dr. Matthew Donahue, for taking a chance on a young aspiring researcher; I truly wouldn't be where I am today without you. Thank you for your continued mentorship and guidance. I would also like to thank the Honors College for allowing me to grow as a leader, mentor, and scholar through 4 years of service. I have met some of the best role models, colleagues, and friends during my time in the HC, and I hope to one day serve in this aspect to another young scholar.

I woud also like to thank all the past and present members of the Donahue Research Group. Thank you for being some of my best friends. I could always talk to you when I was having a rough day, needed a second set of eyes for a spectra, or even to just talk about useless conspiracy theories. You have all been the best part of my college experience.

Finally, thank you to my family, friends, and classmates who have encouraged me along my college journey. To my family, who never had a clue what my research was about, thank you for pretending to listen when I talked for hours-on-end about what probably felt like another language. I really appreciate your endless support and encouragement.

TABLE OF CONTENTS

LIST OF TABLES

LIST OF ILLUSTRATIONS

LIST OF ABBREVIATIONS

COSY	Homonuclear Correlation Spectroscopy
DEPT	Distortionless Enhancement by Polarization Transfer
HMBC	Heteronuclear Multiple Bond Correlation
HPLC	High Performance Liquid Chromatography
HSQC	Heteronuclear Single Quantum Correlation
mCPBA	meta-Chloroperoxybenzoic Acid
NME	New Molecular Entities
NMR	Nuclear Magnetic Resonance Spectroscopy
R&D	Research and Development
SMR	Six-membered Ring
TLC	Thin Layer Chromatography
US FDA	United States Food and Drug Adminstration

CHAPTER I: INTRODUCTION

Nitrogen Heterocycles

Nitrogen-based heterocyclic chemistry is one of the most important and unique branches of synthetic organic chemistry, with research around the subject growing in popularity over the past decade. Being an integral component of over half of all United States Food and Drug Administration (FDA) approved small-molecule drugs, nitrogen heterocycles possess physiological and pharmacological properties that are widely beneficial as structural components of biologically important molecules, such as vitamins, nucleic acids, pharmaceuticals (**Table 1**), antibiotics, dyes, and agrochemicals.[1] In a publication by Vitaku and colleagues from 2014, the authors provided an in depth compilation of the frequency of different types of nitrogen heterocycles among US FDA approved pharmaceuticals, as well as an analysis of the structural diversity and substitution patterns among them. In 2014, there were a total of 1035 FDA-approved unique small-molecule drugs. Among those, 874 molecules have structures that contain a nitrogen atom, with 613 of those molecules containing a nitrogen heterocycle. In addition to the 27 nitrogen-heterocyclic combination drugs (two

Table 1: Nitrogen Heterocycles in Common Pharmaceuticals

Structure	***Drug Name***	***Activity***
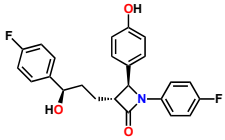	*Ezetimibe*	*cholesterol absorption inhibitor*
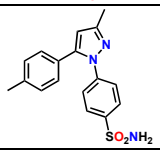	*Celecoxib*	*anti-inflammatory*
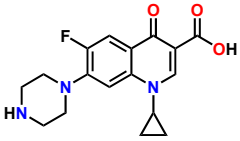	*Ciprofloxacin*	*antibiotic*
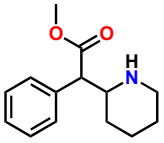	*Methylphenidate*	*stimulant used for ADHD & narcolepsy*

or more active ingredients in single dosage form), there were a total of 640 small-molecule drugs that contain nitrogen heterocycles, making the motif prevalent in 59% of all unique small-molecule drugs.[2] According to the FDA database, there are currently 3,568 domestic US FDA-approved drugs, with 2684 total approved small molecule drugs. Nearly 75% of these unique small molecule drugs contain a nitrogen heterocycle. Moreover, many drug molecules consist of more than one nitrogen per molecule, with the average being 2.3 N/ drug for all small molecule drugs and 3.1 N/ drug for nitrogen heterocycle-containing drugs.[2]

Many heterocyclic scaffolds can be considered privileged structures, which are molecular scaffolds with versatile binding properties.[3] The central role of heterocycles in modern drug design is widely due to recent advances in synthetic methodologies, such as metal-catalyzed cross-coupling and hetero-coupling reactions that allow for rapid access to a wide variety of functionalized heterocycles.[4] Moreover, many heterocyclic pharmaceuticals are isolated from natural resources, with their structures being simplified and modified in the drug manufacturing process.

Within the top 25 most utilized nitrogen heterocycles in US FDA-approved drugs, five six-membered ring (SMR) structures can be found in the majority of drugs: (1) piperidine, (2) pyridine, (3) piperazine, (4) phenothiazine, and (5) pyrimidine (**Table 2**).

Table 2: Top 5 Six-Membered N-Heterocycles

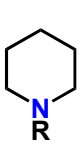	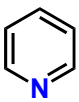	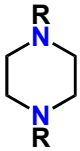	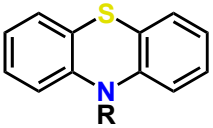	
piperidine	pyridine	piperazine	phenothiazine	pyrimidine

Aromatic rings are a common and very powerful motif in drug discovery due to their unique mode of interaction with target proteins. However, six-membered nonaromatic rings are the most prevalent structure found in all FDA-approved pharmaceuticals, with piperidine and piperazine being the most common.

Piperidines

Piperidines are ranked the most frequent nitrogen heterocycle of all US FDA-approved drugs, making up 72 unique small molecule drugs.[2] Piperidines are SMR structures with five carbon atoms and one nitrogen atom, and have a wide range of practical and therapeutic applications such as antipsychotics and analgesics (**Figure 2**). Piperidines often occupy small molecule pharmaceuticals as a centralized scaffold to which different substituents can be attached (**Figure 1**). The N1 and C4 positions of the piperidine are strongly favored, meaning that they are the most likely to contain a substituent *para* to the nitrogen atom. This is followed by the C2 and C3 positions, and finally the C5 and C6 positions, which are very rarely substituted. Additionally, the piperidine ring is more likely to be disubstituted than monosubstituted, with 1,4-disubstitution occurring 39% of the time.[2] The diversity in the structure and substituting pattern of the piperidine scaffold in pharmaceuticals classifies the structure as a privileged moiety that has the ability to provide potent and selective ligands for a range of different biological targets.[2]

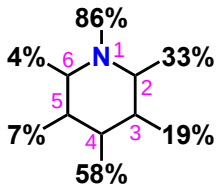

Figure 1: Piperidine Ring Substituent Pattern

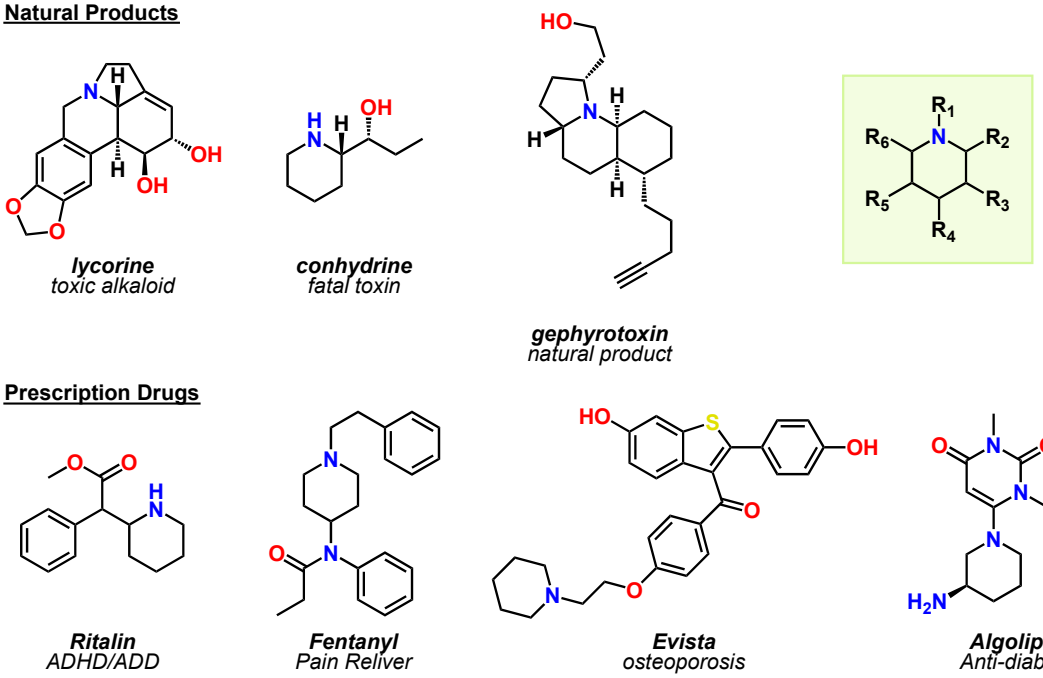

Figure 2: Relevance of Piperidine Scaffold

New Drug Market

A 2016 study stated that global net spending on prescription drugs increased 20% between the years 2013 and 2015, now comprising 17% of total healthcare costs.[5] In contrast to other countries, the United States spends over $800 per capita per year on prescription drugs, as opposed to an average of $400 by other highly industrialized nations.[6] The United States has the highest-grossing revenue for their top 20 prescription drugs, which is almost 3 times greater than that in the United Kingdom.[7] The top 20 best-selling pharmaceuticals account for 15% of global pharmaceutical spending, allowing private pharmaceutical companies such as Pfizer, Roche, and Merck to turn a high profit and monopolize the US pharmaceutical market.[7] Prices for the top brand-name drugs in the U.S. increased by nearly 130% between 2008 and 2014, creating a competitive marketplace that is completely controlled by private companies. Manufacturers aim to

turn a quick profit, and with the US having the highest chronic disease burden and obesity rate, it is almost instantaneous that new drugs in these high-value therapeutic regions will earn a lucrative profit.[8] High drug costs require patients, regardless of their insurance plan, to pay inflated co-payments for their medications, thus affecting immediate and affordable access to prescriptions leading to consequential negative health outcomes.[5] Therefore, the need for new, cost-effective and time-efficient synthetic methodologies to produce precious prescription drug moieties is more prominent than ever.

Due to exorbitant research and development (R&D) costs to bring a new drug to the market, as well as continuing tightening federal regulations, the rate of new pharmaceutical drugs entering the market is slowly decreasing. The average time between clinical testing for a new drug until marketing approval is approximately 97 months or 8 years.[9] The cost of drug development can range anywhere from $157.3 million to $1.95 billion, without considering opportunity costs.[10] Moreover, the total amount of money that pharmaceuticals have contributed to R&D costs consistently increases each year, ranging from $15 billion in 1995 to approximately $40 billion in 2005.[11]

Furthermore, new molecular entities (NME) that were introduced to the market in recent years lack the market revenue stream of previous drugs. From 1990 to 1994, 11 new market drugs reached the top 100 drugs in terms of global revenue.[11] However, from 2000 to 2004, only two new markets drugs were able to receive the distinction of "top 100 drugs." This can be attributed to the fact that only 11.8% of experimental drugs succeed during clinical trials, while a vast majority fall short after several years in development.[11] Market oversaturation and competition have increased the burden on drug

innovation; it is becoming harder to develop a "new" and novel medication that will thrive in the market. Therefore, it is more relevant than ever to discover new synthetic methods for innovative pharmaceutical moieties that are cost-effective and time efficient to capitalize on gross revenue profit, make up for lost revenue of failed drugs, and be able to provide lifesaving drugs to those who may not be able to afford the current market price.

CHAPTER II: BACKGROUND

Iminium Ions

The synthesis of N-heterocycles is growing increasingly popular in recent years, as it is becoming ever important to continue developing new pharmacophores as diseases and viruses continue to emerge and mutate. Equally important to nitrogen heterocycle synthesis is the understanding of iminium ions and their reactivity, spatial arrangement, and electrophilicity in reaction mechanisms. Iminium ion cyclizations, such as the Pictet-Spengler cyclization, are a widely studied area of alkaloid chemistry to create carbon-carbon bonds between the α carbon and the basic nitrogen and an aromatic ring (**Scheme 1**).[12] Iminium ions are obtained by protonation and alkylation of imines but can also be generated by condensation of secondary amines with ketones or aldehydes. These cations adopt alkene-like geometries, in which the C=N unit is coplanar with all four substituents and cis/trans isomers can be observed. Imines and their derivatives play a significant role as key intermediates in many natural processes, especially for synthesis of

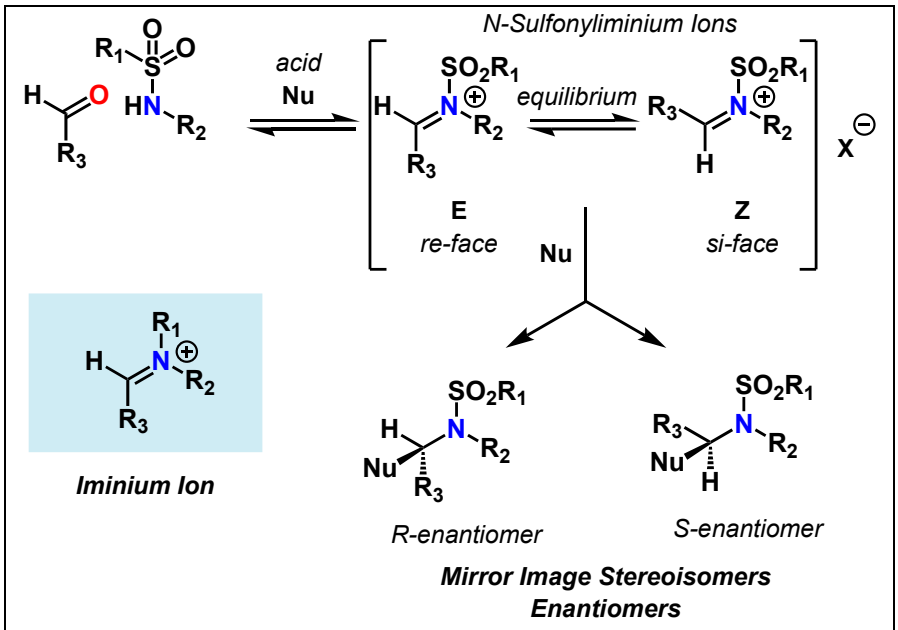

Scheme 1: N-Sulfonyliminium Ion Research Design

nitrogen heterocycles. Many enzymes employ imines as part of their reaction mechanism, such as the coenzyme pyridoxal phosphate (PLP) which forms an imine bond between an amino acid carbonyl group and the amine of lysine.

Enantiomers

One particularly challenging aspect of medicinal chemistry is the formation of stereoisomers. Stereoisomers are molecules that have the same chemical formula but differ in spatial arrangement of their atoms. Specific stereoisomers referred to as configurational isomers are molecules of different configurations that cannot be made superimposed by any rotations around single bonds and can be interconverted only by breaking bonds. Chirality describes a property of a molecule to be asymmetric in the way that its structure and mirror image are inequivalent. This is equivalent to a left hand–right hand relationship, in which each hand is a mirror image of the other and both cannot be superimposed (thumbs will not overlap if both hands are placed palm-up.) Molecules can be considered to have a chiral center if all the surrounding atoms are not equivalent. Enantiomers are configurational stereoisomers that are non-superimposable mirror images of a compound (**Figure 3**).

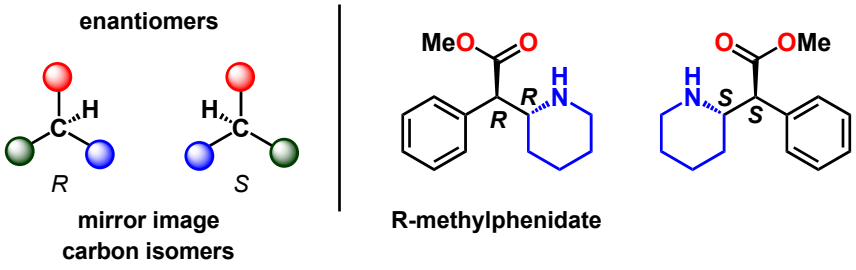

Figure 3: Stereoisomers and Ritalin Example

Enantiomers are pairs of chiral stereoisomers that will have a 1:1 ratio of each pair in a molecule, called a racemic mixture. More than half of the currently marketed pharmaceutical drugs are chiral compounds with almost 90% marketed as racemates consisting of equimolar mixtures of two enantiomers. For example, Ritalin, which is a central nervous stimulant used to treat diseases such as attention deficit disorder, attention deficit hyperactivity disorder, and narcolepsy, is sold as a racemic mixture of both the R and S enantiomer (**Figure 3**). This can be problematic, because many existing routes used to produce piperidines are not stereoselective and yield racemic compounds that may be deleterious due to unknown pharmaceutical activity. One enantiomer of a prescription drug may be the biologically active medicine for a particular disease, while the other enantiomer may be not only inactive but also toxic. Therefore, synthesizing compounds as a single enantiomer is crucial in the synthesis design of new prescription drugs.

CHAPTER III: RESEARCH DESIGN

The overarching goal of this project is to develop a robust catalytic, asymmetric synthesis of piperidine rings from inexpensive petroleum feedstock chemicals. Small molecules derived from nature serve as a rich source of many pharmaceuticals, specifically anticancer agents and antibiotics. My role in this research project mainly focuses on the use of the Pictet-Spengler cyclization and the Aza Prins/Ritter addition mechanism to form these piperidines. By utilizing commercially available aldehydes and sulfonamides, unnecessary costs can be eliminated and the iminium ion's effect on producing a racemic mixture can be explored.

Pictet Spengler Cyclization

In the Pictet-Spengler Cyclization reaction (**Scheme 2**), an amine **1** undergoes cyclization with an aldehyde **2** followed by a ring closure to the tetrahydro isoquinoline **8**. The mechanism begins with the protonation of the aldehyde carbonyl oxygen **2** by the acid, resulting in the oxonium ion, which subsequently is attacked by the sulfonamide nitrogen **1**. After a series of proton transfer steps (**3→4** and **4→5**), a water molecule (**5→6**) is released, which results in a protonated imine intermediate **6-Z or 6-E**. The molecule then undergoes a *6-endo-trig* cyclization

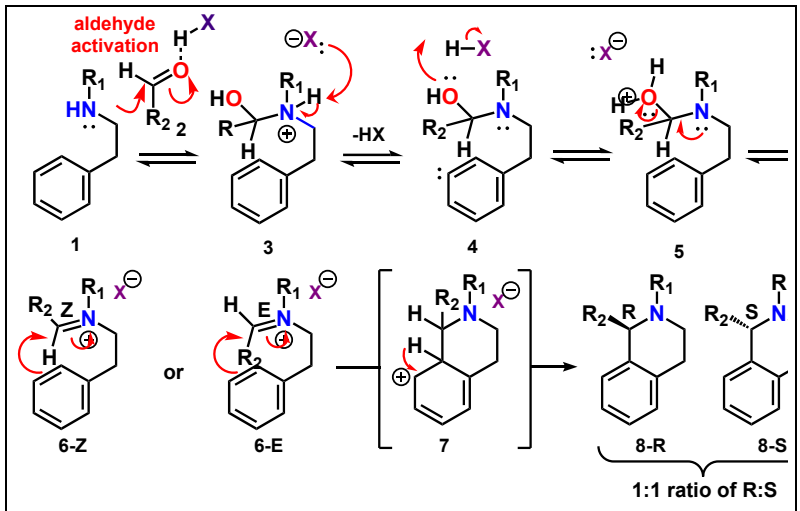

Scheme 2: Pictet-Spengler Cyclization Mechanism

reaction (**6→7**) with loss of aromaticity of the aryl ring. A final deprotonation step by the conjugate base of the acid restores the aromaticity and results in the equal production of tetrahydroisoquinoline products **8-R and 8-S**, a racemic mixture.

This reaction can be modified by adding an electron withdrawing group such as a toluenesulfonyl to the **R1** position on the amine thus removing electron density and making the amine hydrogen more acidic (**Scheme 3**). Acid catalysts are commonly used in this cyclization to further lower the energy difference between the nucleophilic amine and electrophilic aldehyde, causing the electrophilic iminium ion to undergo the reaction. Aldehydes and sulfonamides will condense to form two electrophilic N-sulfonyliminium ions that differ in their relationship across the C=N pi bond, which can be trapped by the aromatic ring system within the molecule. As with Ritalin (**Figure 3**), the two resulting cyclization products are mirror images of one another.

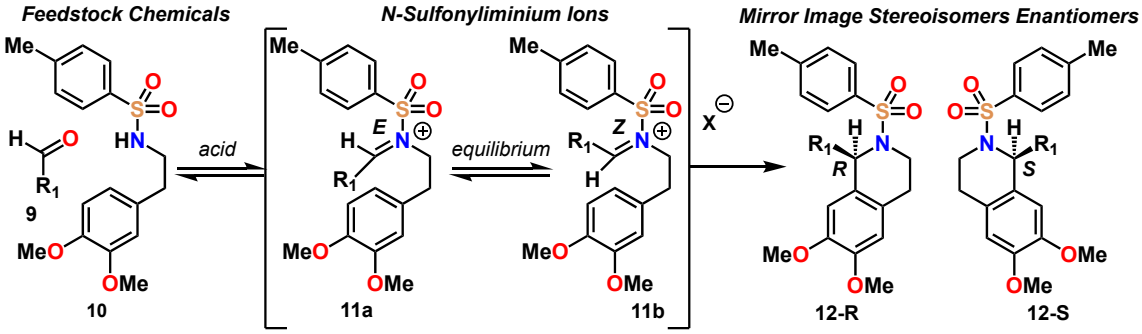

Scheme 3: Research Design for the Synthesis of Nitrogen Heterocycles

Whereas the utility of N-acyliminium ions has been thoroughly investigated, there is little information on the reactivity of the N-sulfonyliminium ion. In theory, nitrogen sulfonamides have inherently low nucleophilicity, making these reactions difficult to proceed in normal conditions. Therefore, when a Lewis acid catalyst is used in

intramolecular cyclization reactions, it bonds to the oxygen atom in aldehydes; this activates the molecule by making the central carbon more electrophilic and allows reactants with low nucleophilicities, such as nitrogen sulfonamides, to undergo nucleophilic attack. Lewis acids such as scandium trifluoromethanesulfonate are highly oxophilic and form a strong but easily altered bond with oxygen atoms. Moreover, they allow the reaction to be carried out in mild conditions with high yields of the final product. The bond between the oxygen-Lewis acid structure eventually breaks, causing the Lewis acid to leave and reforming the catalyst for subsequent reactions.

Homoveratrylamine, also known as dimethoxyphenethylamine (DMPEA), is an analog of the neurotransmitter dopamine in which the 3- and 4- position hydroxy groups have been replaced with methoxy groups. DMPEA occurs naturally in various species of cacti and has some known pharmaceutical activity as a monoamine oxidase inhibitor.[13]

Sulfonamides derived from homoveratrylamine have been shown to cyclize with aldehydes and acetals with Bronsted acids and Lewis acids in non-coordinating solvents. By utilizing para-toluene sulfonamides as opposed to methane sulfonamides, the methyl signature of the toluene allows for easy identification in 1H NMR. Moreover, methyl protons are inherently acidic and can undergo condensation reactions under the proposed conditions. The challenge of this research is controlling the following factors: (i) equilibrium in the formation of the ions **11a** and **11b**; and (ii) the addition of the nucleophile to the face of the iminium ion. *The hypothesis for this project is that transition metal triflates are sufficiently Lewis acidic to activate aldehyde carbonyl groups to undergo attack by relatively inert sulfonamides, triggering the nitrogen for intramolecular cyclization forming piperidines*. Any successful transition metal triflates

will then be screened with various chiral ligands to introduce asymmetry into the cyclization event.

Aza Prins/ Ritter Reaction

The second portion of this project will focus on the Aza Prins/ Ritter reaction of N-sulfonyl homoallylic amines, which gives direct access to the piperidine skeleton with the addition of a nucleophile at the C4 position (**Scheme 4**). The Aza Prins reaction begins with the condensation of homoallylic amine **13** with an aldehyde **14** in the presence of an acid to give an iminium ion **18-Z** or **18-E**, which then undergoes the intramolecular nucleophilic attack by the olefin.[14] A Ritter addition is then performed, in which a nitrile and carbocation precursor will convert to amide **21-R** or **21-S** using a strong acid and water. The reaction proceeds by the electrophilic addition of the carbocation **19** to the nitrile. The resulting nitrilium ion **20** is hydrolyzed by water to the

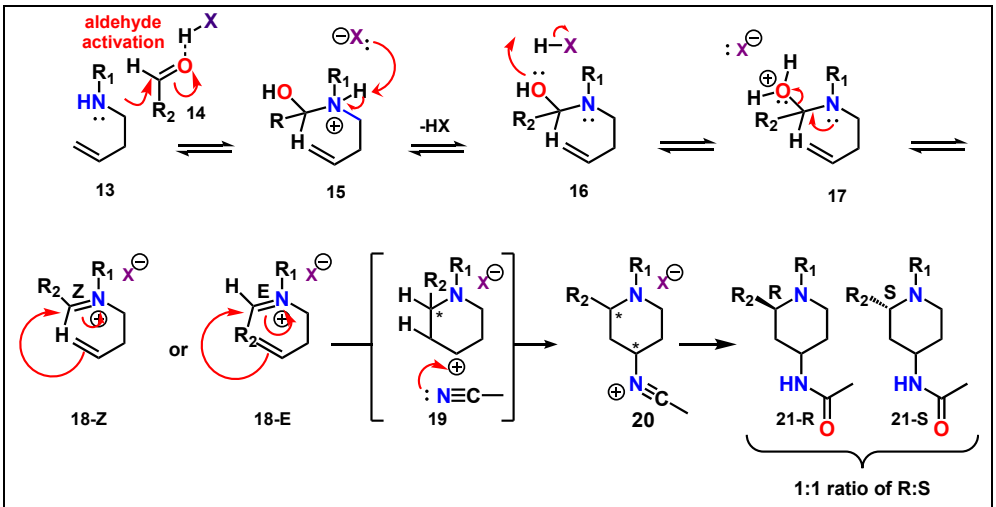

Scheme 4: Aza Prins/ Ritter Mechanism

desired amide.[15] In theory, sulfonamide nitrogen is more nucleophilic than amide nitrogen, due to resonance with the carbonyl oxygen. Both the oxygen and the nitrogen in amides are sp^2 hybridized, which causes the lone pairs on nitrogen to be delocalized and in resonance with the p orbital of the C=O double bond. Amide bonds are very stable due

to the near-perfect overlap of their p orbitals, which significantly reduces the partial positive charge on the carbonyl carbon, thus making it less electrophilic. Therefore, *the hypothesis for this project is that secondary sulfonamides should readily condense with electrophilic aldehydes in the presence of acid to generate an N-sulfonyliminium ion*.

CHAPTER IV: GENERAL LABORATORY TECHNIQUES

Materials

Starting materials were purchased from commercial vendors and checked for identity and purity using IR, NMR and HPLC and were used without purification unless noted.

Methods

To monitor reaction conversion and progress, we employed the use of thin-layer chromatography (TLC), high-performance liquid chromatography (HPLC), and nuclear magnetic resonance spectroscopy (NMR) as analytical methods. Solvent removal was effected using a Buchi R3 rotary evaporator with a V900 diaphragm pump (~ 10 mmHg). All yields refer to isolated material that is chromatographically (TLC or HPLC) and spectroscopically (^{1}H NMR) homogeneous. Further descriptions of individual methods and how they were utilized have been included below.

Pictet-Spengler Methods

All reactions were left to stir for 24 hours and monitored via TLC (100% dichloromethane) on regular phase silica gel by observing the disappearance of the sulfonamide spot in the reaction mixture lane. The piperidine product formed a new spot at Rf 0.58, with excess aldehyde and acid catalyst also being observed towards the solvent line. Upon completion, the reaction mixture was diluted with dichloromethane (DCM) and saturated aqueous sodium carbonate and stirred vigorously for one hour. The organic layer was then separated, dried with magnesium sulfate, and gravity filtered before concentration via rotary evaporator. The reaction mixture was then analyzed by ^{1}H NMR to determine the percent conversion and identify the product.

Aza Prins/Ritter Methods

The reaction was monitored via TLC (4:1 hexanes-ethyl acetate) on regular phase silica gel and then quenched upon completion with 1N HCL and left to stir for 1 hour. The organic phase was then separated, dried with magnesium sulfate and vacuum filtered. The reaction mixture was analyzed by ^{1}H NMR to calculate conversion and determine the reaction product.

Thin Layer Chromatography

Thin layer chromatography (TLC) is a chromatographic technique used to separate components of a mixture using differences in the components' affinities for the mobile and stationary phases. TLC plates (chromatoplates) made of silica gel act as the stationary phase, while a solvent of choice acts as the mobile phase. The choice of solvent used in TLC is guided by two factors: the polarity of the constituents to be separated and the nature of the process involved. The retention factor (Rf) describes the ratio of the distance migrated of a compound over the total distance of the solvent. Considering the Rf value is a ratio, individual compounds will have unique Rf values independent of the mobile phase. When comparing two different compounds under the same conditions, the compound with the larger Rf value is less polar because it is carried by the mobile phase a longer distance, while the smaller Rf value is more polar because it "sticks" to the stationary phase and is carried a shorter distance (**Figure 4**).

On an analytical scale, TLC can be used to monitor the progress of a reaction by observing the appearance of a product or disappearance of a reactant at different points in the reaction progress. Typical TLC plates have three lanes: the reactant, the reaction mixture, and a "cospot" where the reaction mixture is spotted directly on top of reactant. Small aliquots (10^{-6} g) of a sample can be analyzed by TLC to monitor reaction conversion at distinct time intervals and give insight to the progress of a reaction. Analytical thin layer chromatography was performed using Sorbent Technologies 250 μm glass-backed UV254 silica gel plates. The plates were first analyzed under 254 nm irradiation by UV light, then stained with phosphomolybdic acid followed by heating.

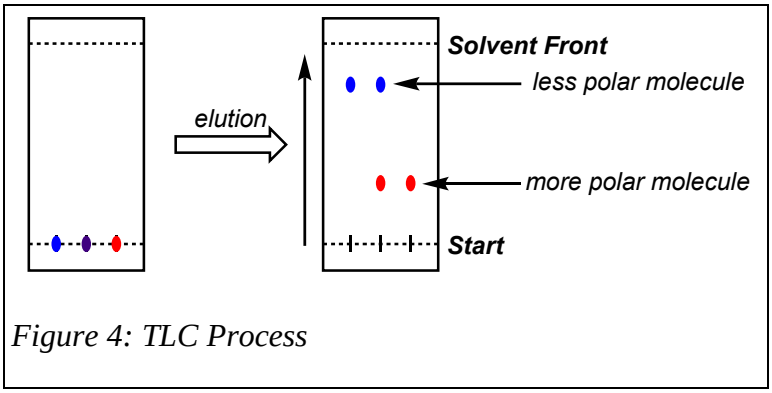

Figure 4: TLC Process

High Performance Liquid Chromatography

High Perfromance Liquid Chromatography also uses the principle of chromatography to separate components of a mixture based on polarity; however, this technique offers more resolution and computer integration to quantitively measure the reaction progress. Mechanical pumps are used to pump pressurized liquid (mobile phase) into the system and an injector introduces the sample into the mobile phase. The sample then enters the column (stationary phase) at a constant flow rate, and the mobile phase acts as a carrier through the column. A compound that is more polar will adhere to the stationary phase, thus eluting from the column later than compounds that are less polar.

This method is used to separate biproducts, intermediates, starting material, and major products from the reaction mixture.

Nuclear Magnetic Resonance Spectroscopy

Nuclear Magnetic Resonance Spectroscopy (NMR) has become the preeminent technique for determining the structure of organic compounds by observing local magnetic fields around atomic nucleic. The principle of NMR is that nuclei of elemental isotopes have characteristic spins that are electrically charged. This spinning generates a magnetic field that has a magnetic moment **(μ)** proportional to the spin. In the presence of an external magnetic field (β_0), energy transfer occurs between the base energy to a higher energy level, causing energy to be emitted when the spin returns to base level. Two spin states exist, with the magnetic moment of the lower energy state aligned to the external field, and the higher energy spin state opposed to the external field. For spin ½ nuclei, the energy difference between the two spin states at a given magnetic field is proportional to their magnetic moments. For common nuclei, such as ^{13}C, ^{1}H, and ^{19}F, the spin state energy separations can used to predict their approximate frequencies. The NMR spectrometer can differentiate between elements and isotopes because the specific nuclei will absorb at different frequencies, meaning that NMR can be "tuned" to specific nuclei. In this project, we will solely utilize ^{13}C, ^{1}H, and two-dimensional NMR techniques on a 400 MHz NMR for the analysis of organic molecules and measurement of conversion from starting material to product.

The principle behind proton NMR (^{1}H NMR) is that each unique hydrogen nuclei in a compound exhibits a predictable precession in a magnetic field. This generates a calculatable peak on the computerized spectrum, which can be used to elucidate the

structure of compounds in a sample. Hydrogens in different chemical environments will resonate at slightly different frequencies, causing them to "shift" on the spectra. This is a result of the atom's nucleus being either deshielded (downfield shift) or shielded (upfield shift) (**Figure 5**). Two main factors influence chemical shift: (1) deshielding effects due to reduced electron density, and (2) anisotropy (due to magnetic fields generated by π bonds). Chemical shifts can be used to identify structural properties in a molecule by analyzing differences in chemical environments. Moreover, integration can be used to identify the relative ratio of H atoms that a peak represents

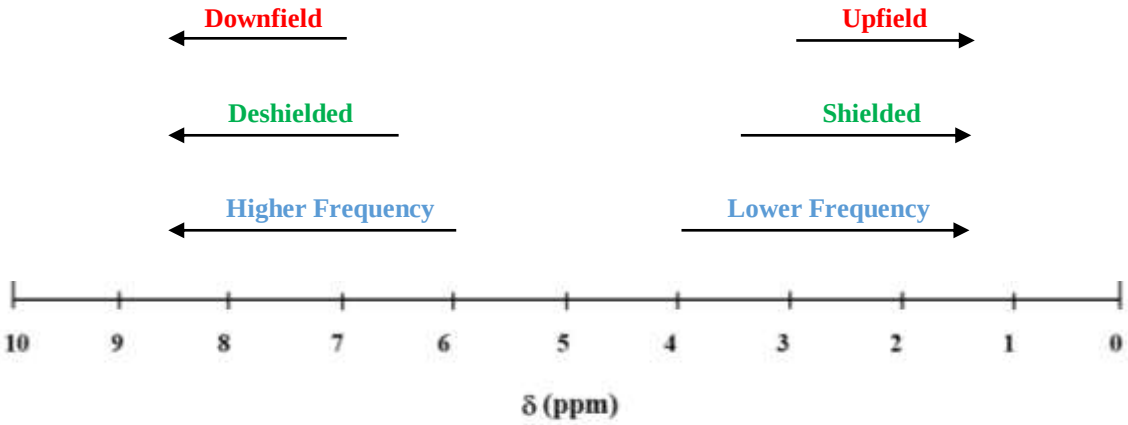

Figure 5: NMR Chemical Shift

Unlike ^{1}H NMR, there is no integration and signal splitting in ^{13}C NMR, due to the low natural abundance (1%) of the ^{13}C isotope. In consequence, carbon NMR signals are relatively weaker and no carbon-carbon splitting is observed. However, proton-carbon splitting by neighboring hydrogens does occur, which often leads to complicated splitting patterns. Due to this effect, a proton-decoupled NMR is commonly used, which eliminates the signal splitting and reduces the ^{13}C peaks to individual singlets. Following this experiment, two distortionless enhancement by polarization transfer (DEPT) are run to determine the multiplicity of carbon nuclei (primary, secondary or tertiary.) DEPT135

experiments differentiate between CH, CH_2, and CH_3 groups by orienting the CH and CH_3 peaks **up** while CH_2 peaks point **down**. To differentiate between CH and CH_3 peak, a second experiment called DEPT90 is used to isolate the CH peaks exclusively, allowing for the identification of CH peaks from the DEPT135 spectra.

Two-dimensional NMR techniques such as homonuclear correlation spectroscopy (COSY), heteronuclear single quantum correlation (HSQC), and heteronuclear multiple bond correlation (HMBC) were also used in the elucidation of structures. COSY correlates chemical shifts of coupled hydrogen nuclei between vicinal protons. The ^{1}H NMR spectra is plotted both axis, which reveals information about the scalar coupling and can help resolve the structure of the molecule. On the other hand, HSQC is used to determine proton-carbon single bond correlations. The resulting spectrum has one axis for proton (^{1}H) and one axis for carbon (^{13}C), resulting in a peak for each unique proton attached to a heteronucleus. HMBC experiment give correlations between carbons and protons that are separated by multiple bonds, much like proton-proton connectivity in COSY. This spectrum is similar to HSQC in that the horizontal axis bears the ^{1}H NMR and the vertical axis bears the ^{13}C NMR, but the proton-carbon cross-peaks are generated from ^{1}H - ^{13}C correlations two, three, and four-bond distances away. The intensity of the cross peaks depends on the coupling constant, which follows the Karplus relationship. This allows for chains of atoms and their overlapping partners to be elucidated from one proton signal, and consequently, the chemical structure can be identified.

Proton nuclear magnetic resonance spectra were recorded on a Bruker UltraShield Plus 400 MHz spectrometer and are recorded in parts per million from internal chloroform (7.26 ppm) on the δ scale and are reported as follows: chemical shift

[multiplicity (s=singlet, d=doublet, t=triplet, q=quartet, qu=quintet, m=multiplet), coupling constant(s) in hertz, integration, interpretation]. 13C NMR data were recorded on a Bruker UltraShield Plus 400 MHz spectrometer and are reported as follows: chemical shift (multiplicity as determined from DEPT (CH, CH3 up and CH2 down) and/or HSQC experiments.

After elucidation of the structure by NMR, each product sample was placed into a Fourier-transform infrared spectrometer (FTIR) equipped with an attenuated total reflectance (ATR) attachment to measure the absorption of electromagnetic radiation. FTIR is a technique used to obtain an infrared spectrum of the absorption or emission of a solid, liquid or gas by using Fourier transform (a mathematical process) to convert raw data into spectra. ATR is a sampling technique used alongside infrared spectroscopy to qualify the sample to be observed directly in the solid or liquid state. FTIR relies on the basis that when introduced to infrared radiation, molecules will vibrate. Covalent bonds will absorb and vibrate at a specific frequency, allowing for the identification of potential functional groups. FTIR spectrometers simultaneously collect high-resolution data over a broad spectrum, which proves significant advantage as opposed to a dispersive spectrometer, which measures intensity over a narrow range of wavelengths at a time.[16] This method allows for the identification of specific functional groups within the molecule, further aiding in the elucidation of chemical structures.

High resolution mass spectrometry (HRMS) can be used to distinguish between compounds of the same nominal mass, determine elemental compositions, and identify unknowns.[17] Mass spectrometry measures the mass-charge ratio (m/z) of an analyte by accelerating positive-charged ionized molecules and deflecting them by a magnetic field.

The beam of ions passing through the machine is then detected, and fragmentation of the molecule are recorded at their corresponding m/z. These fragments act as "puzzle pieces"to help identify the structure of the compound. High-resolution mass spectra were recorded either the Old Dominion University College of Science Major Instrumentation Center (COSMIC) on a Bruker 12 Tesla APEX-Qe FTICR-MS with an Apollo II ion source.

CHAPTER V: RESULTS

Acid Screen of Pictet-Spengler Cyclization with Sulfonamides

To begin the synthetic route, we examined Lewis acids, specifically metal triflates as promoters in the formation of N-sulfonyliminium ions. Recent studies have examined the strong electron-withdrawing ability of triflates to produce an electron-deficient metal cation, which renders strong Lewis acidity for the activation of the aldehyde C-O double bond.[18] N-para-toluenesulfonyl homoveratrylamine **10** was reacted with the test aldehyde 3-phenylpropanal **22** and screened against different metal triflates to determine the steric effect of the sulfonamide moiety on imine activation.

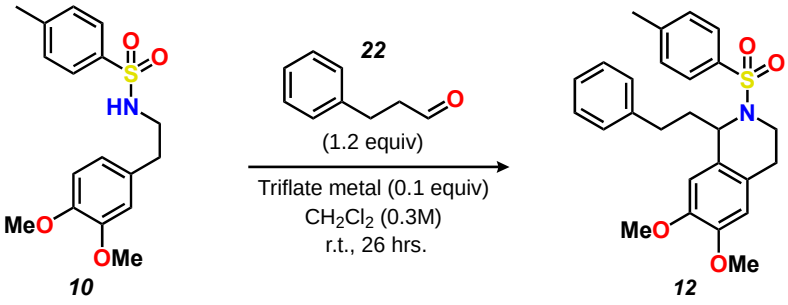

Scheme 5: Pictet-Spengler Cyclization with 3-Phenylpropanal

Initial results showed fastest and complete conversions to the cyclized piperidine product with Sc^{3+}, Sn^{2+}, and Cu^{2+} triflates. Meanwhile, triflates of alkali and alkaline earth metals, such as Na^{+} and Mg^{2+} gave little to no conversion to the piperidine product under the allotted time (24 hrs.) The fastest conversions were observed in polar non-coordinating solvents such as dichloromethane, compared to non-polar solvents such as hexanes and toluene. Solvents such as ether or tetrahydrofuran containing lone-paired oxygen resulted in sluggish conversions, presumably due to the oxygen coordinating with the electrophilic metal.

Based on NMR verification, ring closure to the tetrahydroisoquinole product occurred at the ortho position, which showed a characteristic proton peak at ~ 4.98 ppm (**Figure 7**). This peak appeared as a doublet of doublets (dd), which is due to the ^{3}J coupling of the neighboring diastereotopic CH_2 group in the ethylbenzene chain. Further, the original sulfonamide **10** showed three aromatic protons in the dimethoxy benzene ring: one doublet of doublets (6.62 ppm) and two doublets (6.72 ppm; 6.57 ppm), while

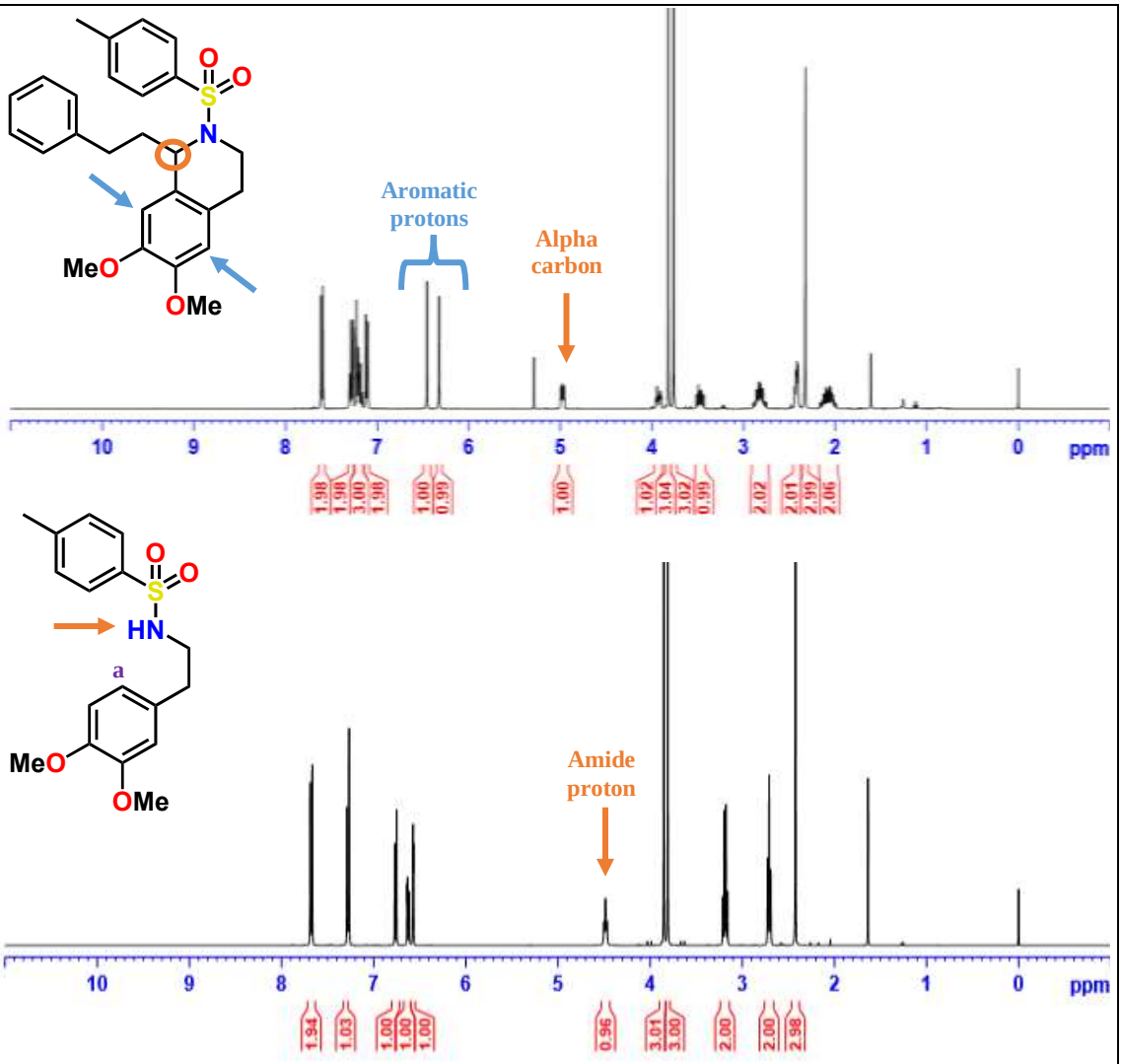

Figure 8: 1H NMR Stack Plot of Tetrahydroisoquinoline Product vs. Homoveratrylamine

the cyclized product showed only two singlets at 6.45 ppm and 6.32 ppm, thus indicating the loss of *meta*-coupling by proton **a**.

Investigation of N-sulfonyl Group of Homoveratrylamine

Upon finding that metal triflates are successful acid catalysts in the cyclization, a derivation of the sulfonamide group was investigated to determine the substitution effects on the cyclization (**Scheme 6**). Preparation of the new sulfonamides was conducted by the tosylation of homoveratrylamine with R-substituted sulfonyl chloride in the presence of triethylamine (TEA) and DCM.

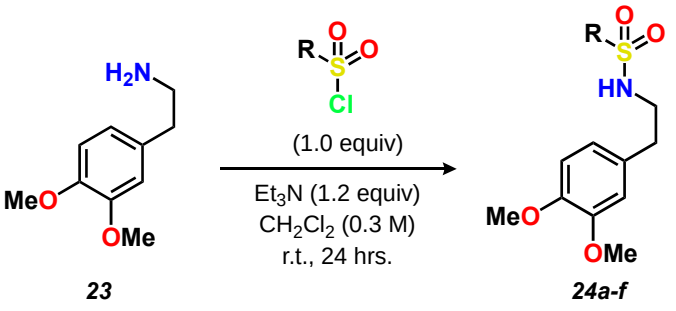

Scheme 6: N-Sulfonyl Group Screen

Further studies examined how the N-sulfonyl group influenced conversion to the tetrahydroisoquinoline product. Scandium (III) triflate was used as the Lewis acid catalyst (0.1 equivalent) for the cyclization of the N-sulfonamides **24a-f** with 3-phenylpropanal **22** in the presence of DCM at room temperature. All reactions were left to stir for 24 hours and were monitored via TLC for reaction completion. ^{1}H NMR allowed for analysis of conversion by calculating the ratio of the aromatic dimethoxy protons, as well as the disappearance of the sulfonamide NH peak. Results found that sulfonamides containing heteroatoms showed little to no conversion to the piperidine product, presumably due to competition with the aldehyde as a Lewis base (**Figure 9**).

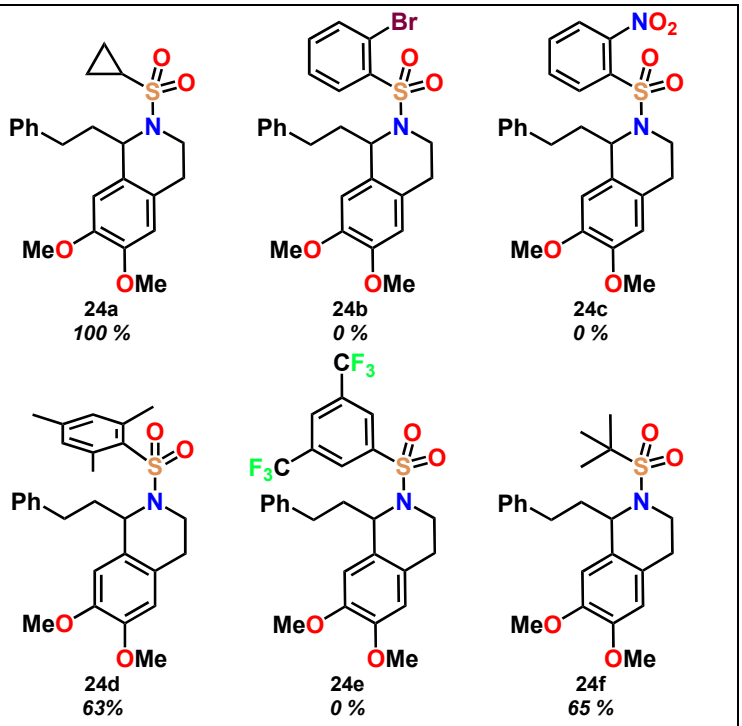

Figure 9: Results of N-sulfonyl Group Screen with 3-phenylpropanal

Heteroatoms are any group that is not carbon or hydrogen, and in the case of nitrogen, oxygen, bromine, and fluorine, they can act as proton acceptors causing the acid to protonate at the heteroatom substituent rather than the aldehyde oxygen. Only sulfonamides with carbon-based substituents were shown to perform the cyclization, except for sulfonamide **24f,** which showed decreased conversion due to the steric hindrance of the tert-butyl group. Steric hindrance is the prevention of inter- or intramolecular interactions as a result of the spatial structure of a molecule.

Aldehyde Screen of Pictet-Spengler Cyclization with Sulfonamides

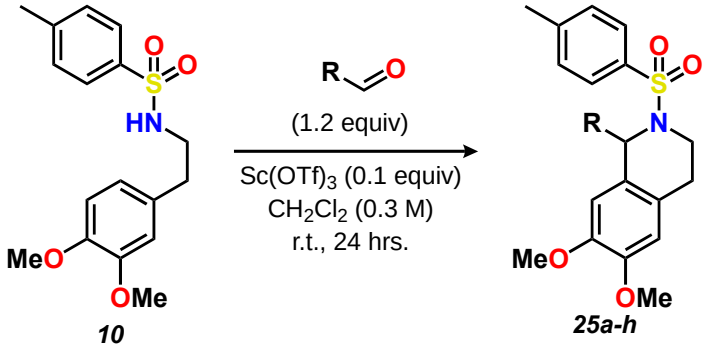

Scheme 7: Aldehyde Screen of Pictet-Spengler Cyclization

Considering that activation of the aldehyde is the initial step of the cyclization, a substrate screen of aldehydes was performed to test the steric effects of changing the "R" substituent at the alpha carbon on aldehyde reactivity. Both enolalizable and non-enolizable aldehydes were examined to determine if the high reactivity of the electron-rich enol form is a major contributor to the cyclization event, or if the reaction can proceed through a non-activated keto form. Many aldehydes have a neighboring carbon

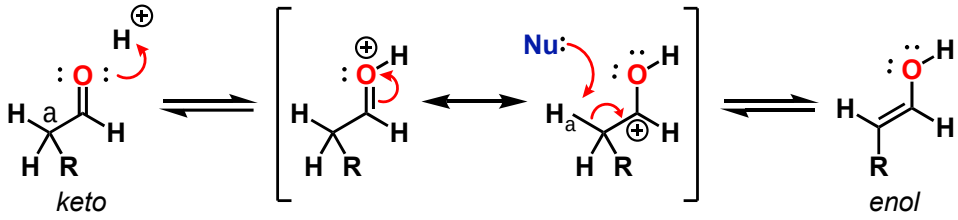

Scheme 8: Mechanism for Keto-Enol Tautomerism

bearing at least one hydrogen atom, referred to as the alpha hydrogens. These hydrogens can be removed easily through resonance stabilization, which causes the negative charge to be shared between the alpha carbon and the oxygen, forming an enol. However, if

there are no alpha hydrogens attached, the enol cannot form, and the reaction may proceed differently.

In this screen, aldehydes of varying carbon chain lengths and substituents were reacted with N-paratoluene homoveratrylamine with $Sc(OTf)_3$ (0.1 equiv) in the presence of DCM. Initial results found that sp^3 carbons next to the aldehyde were successful in performing the cyclization, while sp^2 carbons next to the aldehyde were not successful (**Figure 10**). This means that the activation of the aldehyde from keto to enol form is necessary in the cyclization event to provide an electrophilic carbon center for the nucleophilic nitrogen to attack. Exceptions include pivalaldehyde **25h,** which could be recalcitrant to the cyclization due to the steric hindrance caused by the bulkiness of the tert-butyl group

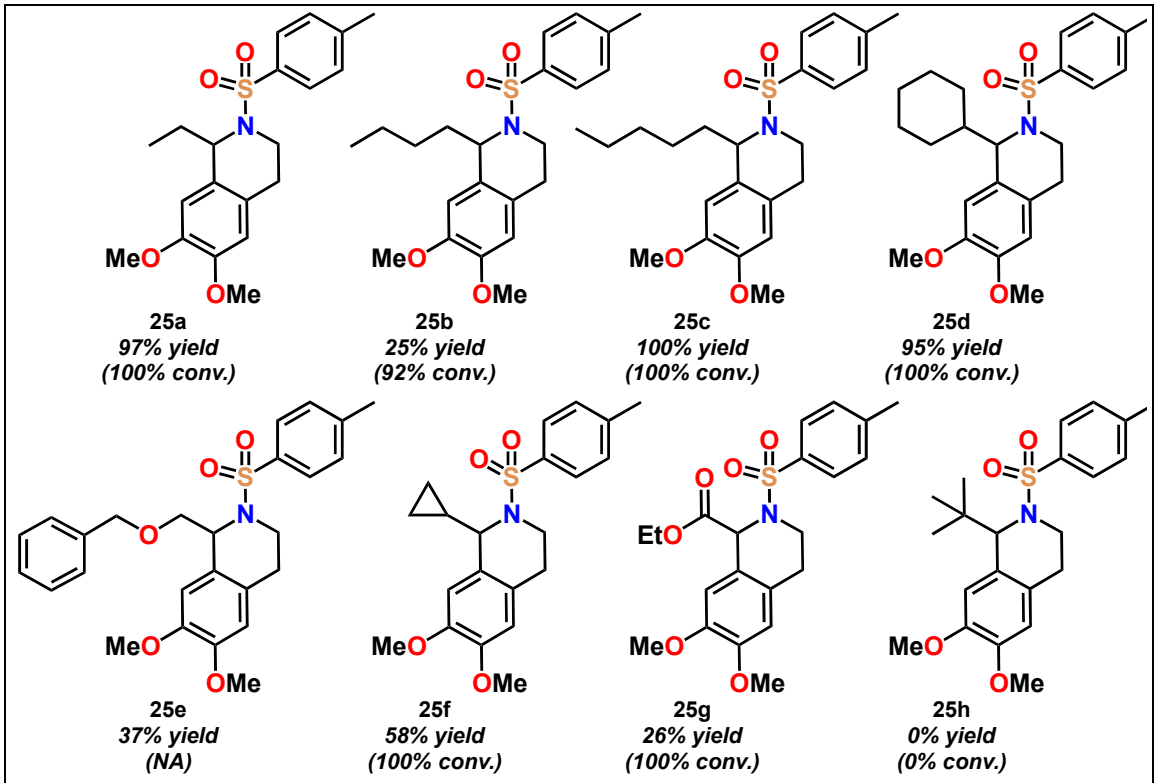

Figure 10: Tolerance of Aldehyde Group

Acid Screen of Aza Prins/Ritter Reaction

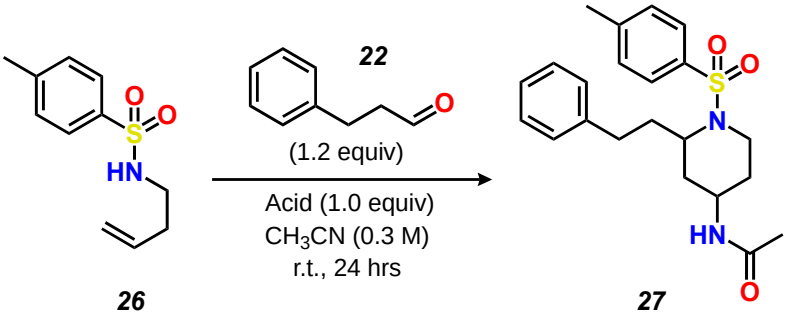

Scheme 9: Acid Screen of Aza Prins/Ritter Reaction

To test the hypothesis that N-sulfonyl homoallylic amines will readily condense with aldehydes, an acid catalyst screen was performed with both Bronsted-Lowry acids and Lewis acids as promoters for the formation of the N-sulfonyliminium ion. N-tosyl homoallylic amine **26** was coupled with 3-phenylpropanal **22** in the presence of 1.0 equivalence of test acid and acetonitrile at room temperature.

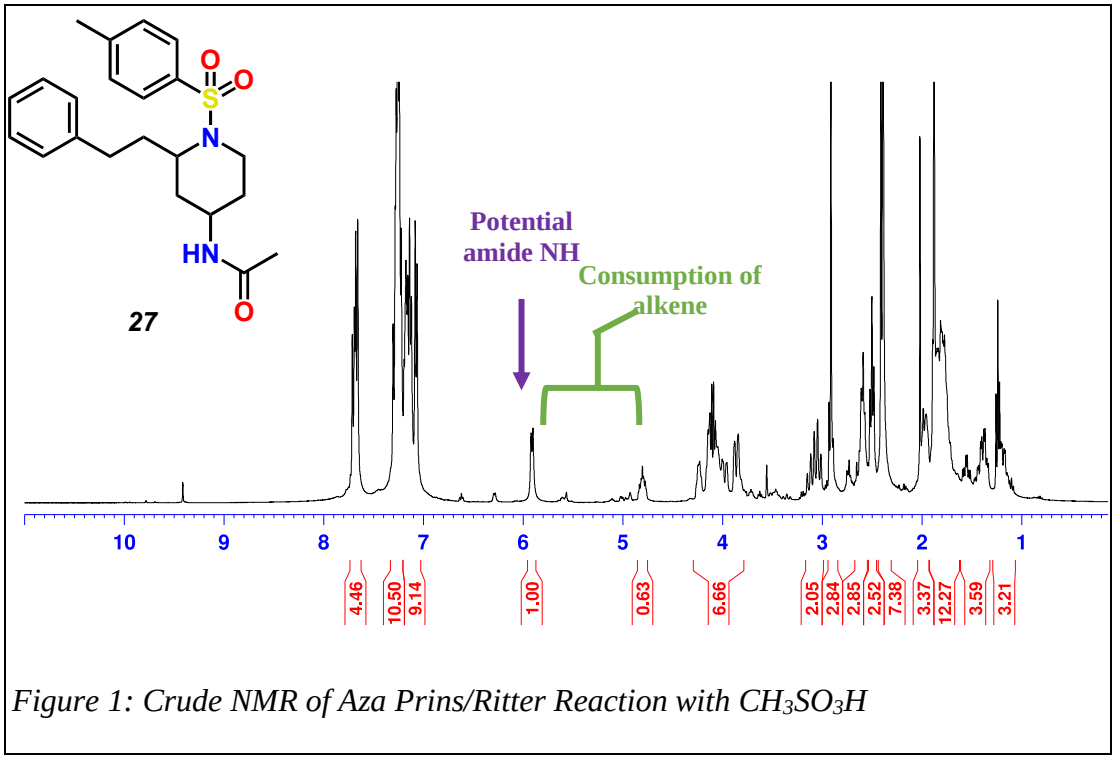

Figure 1: Crude NMR of Aza Prins/Ritter Reaction with CH_3SO_3H

The crude sample was then analyzed by ^{1}H NMR (**Figure 11**), which showed several new peaks at 5.9 ppm, 4.8 ppm, and 4.2 ppm that were indicative of the N-tosyl piperidine amide formation shown in **Scheme 9**. The disappearance of the peaks at 5.6 ppm, 5.1 ppm, and 4.5 ppm were indicative signals of a successful cyclization, although resolving the peaks were near impossible in the current conditions. It was anticipated that the cyclization would not be stereoselective and the generation of diastereomers would be observed, resulting in a remarkably complex ^{1}H NMR. However, the complication of the crude spectrum gave insight that another product was being formed in the addition reaction and that purification was needed to separate the two products.

Initial results of the acid screen showed that strong Bronsted acids produced the best conversion to the piperidine product as compared to weak Bronsted acids (**Figure 12**). In general, strong Bronsted acids have relatively small or negative pKa values,which measures how tightly protons are "held" by the molecule. The lower the pKa value, the more H^{+} ions will dissociate in solution, and the stronger the proton donator. Sulfonic acids **28a-d** are very strong Bronsted acids because their conjugate bases (sulfonate anions) are resonance stabilized, which delocalizes the negative charge on oxygen. As compared to carboxylic acids, sulfonic acids are

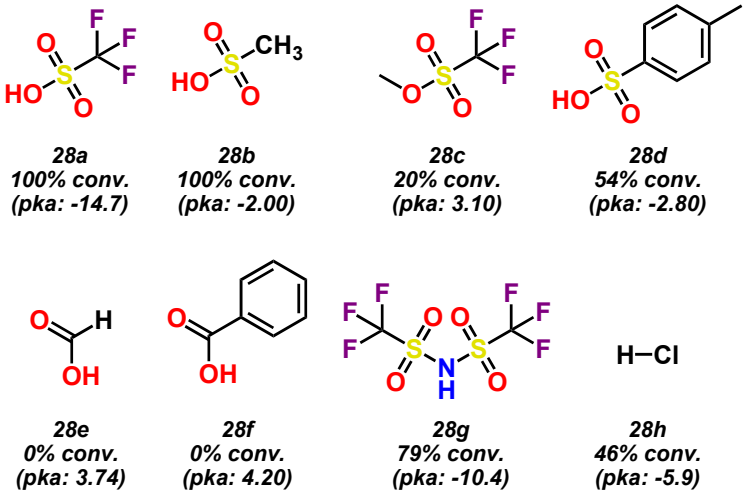

Figure 12: Bronsted Acid Screen Results of Aza-Prins/Ritter Reaction

inherently “stronger,” due to their number of resonance-stabilized conjugate bases. From this methodology, as well as the pKa values listed in **Figure 12**, we can infer that stronger acids more readily protonate the aldehyde for activation, thus allowing for the formation of the N-sulfonyliminium ion.

Based on success from the Pictet-Spengler reaction, metal triflates and metal chlorides were examined to determine if Lewis acid catalysts are able to coordinate to the nucleophilic carbonyl oxygen to protonate the aldehyde for activation. Lewis acidity measures the strength of an acid by the tendency of the compound to accept a pair of electrons. Lewis acids contain an empty orbital that is capable of accepting an electron pair from a Lewis base, which has a filled bonding orbital containing an electron pair in a nonbonding orbital. Preliminary results indicated that in 0.1 equivalence, only $Sc(OTf)_3$ was able to give modest conversion (30%) to the piperidine product, while $Cu(OTf)_3$, $FeCl_3$, $GaCl_3$, and $NbCl_5$ showed no conversion. It was hypothesized that the low concentration of acid may influence the availability of free orbitals for the carbonyl oxygen to coordinate to. A second screen was then performed with 0.2 equiv of acid catalyst and 1.0 equiv. of 3-phenylpropanal to increase the ratio of free orbitals to available electrons. ^{1}H NMR analysis showed a slight overall increase in percent conversion for all screened acids (> 40% conversion); however, much of the reaction mixture was still starting material, indicating that the reaction was not proceeding successfully towards the piperidine product.

Comparing the results of the two acid screens, Bronsted acids were much more successful in activating the aldehyde for cyclization. This may be explained by pKa arguments, in which a Bronsted acid becomes negatively charged once deprotonated by

the aldehyde. This negatively-charged conjugate base is present in solution and is later used in the deprotonation of the ammonium ion **15**. If the acid is unable to protonate the aldehyde, the carbonyl carbon becomes less electrophilic and may not be attacked by the amine reagent. Moreover, if deprotonation of the ammonium ion does not occur, the reaction can proceed in the reverse direction and reform the starting material.

Ritter Additions vs. Acid Additions

Proton NMR analysis indicated a surprising byproduct from the Ritter addition of the acetonitrile. The crude NMR showed an unexpected proton peak ~ 4.8 ppm, as well as high-value integrations that did not correlate to the expected hydrogen count. The reaction mixture was then purified by High Performance Liquid Chromatography (HPLC) which allowed for separation of the piperidine product and the cyclization byproduct. The two samples were characterized by ^{1}H NMR, ^{13}C NMR, 2D NMR, and mass spectrometry to identify their chemical structures.

Analysis showed that the byproduct of the reaction was due to the acid catalyst adding *para* to the amine nitrogen at the secondary carbocation formed from the Aza Prins reaction (**Figure 13**). Excess conjugate base in solution can attack the electrophilic carbocation by donating a pair of electrons in the nonbonding orbital to the empty bonding orbital of the carbocation. The ^{1}H NMR spectra of the acid-addition product showed a characteristic proton peak at 4.8 ppm, which corresponds to the proton at the C4 position of the piperidine ring (**Figure 14**). This proton appears more downfield in the acid-addition spectra compared to those from the

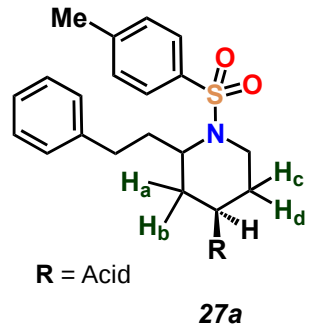

Figure 13: Acid Addition Product

Ritter addition due to the electronegativity of the neighboring heteroatom of the acid, which pulls electron density away from the proton.

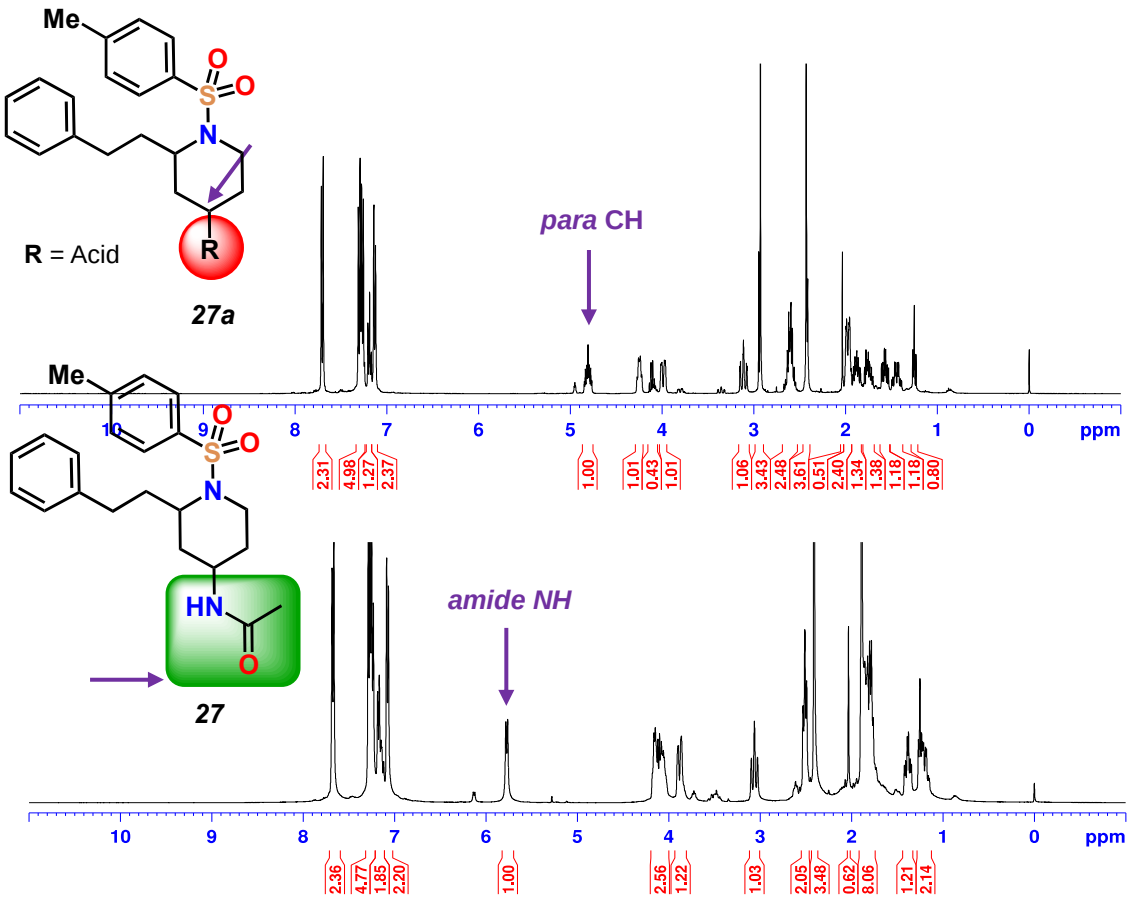

Figure 14: Acid Addition vs. Ritter Addition

Moreover, the Ritter addition product showed a doublet NH amide peak at 5.78 ppm, which is predictably absent from the acid-addition product spectra. Since the C4 proton in the acid-addition product has four neighboring diastereotopic protons, Pascal's triangle results in the equation $2^4 = 16$ meaning that the C4 signal is split into 16 peaks. However, the equatorial-axial and axial-axial couplings of the two neighboring CH_2 groups are similar in nature. The ^1H NMR cannot destinguish between the two as individual peaks, resulting in a triplet of triplets. The 4.6 Hz coupling observed is

characteristic of equatorial-axial coupling from protons H_a and H_d. However, the larger triplet is characteristic of axial-axial coupling (J = 11.6 Hz) from H_b and H_c, indicating that the C4 proton has to be axial (**Figure 15**). If the proton were equatorial, we would only see axial-equatorial and equatorial-equatorial couplings, which are very similar and small couplings and may result in complex splitting.

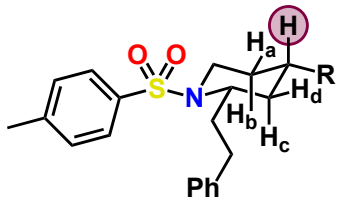

Figure 15: Acid Addition Chair Conformation

CHAPTER VI: Future Work

These preliminary results have produced racemic mixtures of piperidines (**12R:12S)** as standards for future studies that will focus on the use of chiral ligands such as metal PyBox complexes **28 (Figure 16)** to induce asymmetry in the cyclization event.[i] The PyBox ligand has a symmetry element that will discriminate between the *Re* and *Si* face of the *N*-sulfonyliminium ion in the chiral pocket during the cyclization event. By introducing chirality into the cyclization, we will be able to synthesize only one enantiomer of the piperidine ring, rather than both, similar to how enzymes catalyze biochemical stereospecificity. This method has far-reaching societal implications as many FDA approved prescription drugs are single enantiomer molecules. The scientific intellectual caliber of this project will allow for fundamental understanding of how small molecule "chemozymes" such as **29** desymmetrize achiral molecules such as **10** in cyclization reactions.

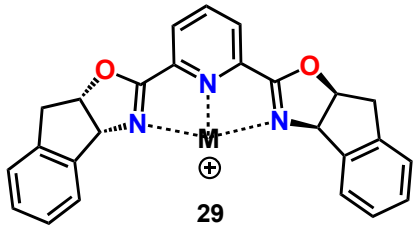

29

Figure 16: PyBOX Chiral Ligand

Additional future studies will investigate the mechanistic route of the acid-addition product, by performing the Aza Prins/Ritter addition in a non-participatory solvent such as DCM. This will eliminate the possibility of amide formation, allowing for the acid catalyst to add to the secondary carbocation without competition. Full characterization of the acid-addition product can then be performed, as well as isolation of the crystalline structure.

REFERENCES

(1) Kerru, N.; Gummidi, L.; Maddila, S.; Gangu, K. K.; Jonnalagadda, S. B. A Review on Recent Advances in Nitrogen-Containing Molecules and Their Biological Applications. *Molecules* **2020**, *25* (8). https://doi.org/10.3390/molecules25081909.

(2) Vitaku, E.; Smith, D. T.; Njardarson, J. T. Analysis of the Structural Diversity, Substitution Patterns, and Frequency of Nitrogen Heterocycles among U.S. FDA Approved Pharmaceuticals: Miniperspective. *J. Med. Chem.* **2014**, *57* (24), 10257–10274. https://doi.org/10.1021/jm501100b.

(3) DeSimone, R.; Currie, K.; Mitchell, S.; Darrow, J.; Pippin, D. Privileged Structures: Applications in Drug Discovery. *CCHTS* **2004**, *7* (5), 473–493. https://doi.org/10.2174/1386207043328544.

(4) Jampilek, J. Heterocycles in Medicinal Chemistry. *Molecules* **2019**, *24* (21), 3839. https://doi.org/10.3390/molecules24213839.

(5) Kesselheim, A. S.; Avorn, J.; Sarpatwari, A. The High Cost of Prescription Drugs in the United States: Origins and Prospects for Reform. *JAMA* **2016**, *316* (8), 858. https://doi.org/10.1001/jama.2016.11237.

(6) *Health at a Glance 2015 OECD Indicators*; OECD., 2015.

(7) How the U.S. Pays 3 Times More for Drugs https://www.scientificamerican.com/article/how-the-u-s-pays-3-times-more-for-drugs/ (accessed 2021 -10 -11).

(8) U.S. Health in International Perspective: Shorter Lives, Poorer Health. *Military Medicine* **2016**, *181* (9), 945–946. https://doi.org/10.7205/MILMED-D-16-00227.

(9) DiMasi, J. A.; Grabowski, H. G.; Hansen, R. W. Innovation in the Pharmaceutical Industry: New Estimates of R&D Costs. *Journal of Health Economics* **2016**, *47*, 20–33. https://doi.org/10.1016/j.jhealeco.2016.01.012.

(10) Prasad, V.; Mailankody, S. Research and Development Spending to Bring a Single Cancer Drug to Market and Revenues After Approval. *JAMA Intern Med* **2017**, *177* (11), 1569. https://doi.org/10.1001/jamainternmed.2017.3601.

(11) Hu, M.; Schultz, K.; Sheu, J.; Tschopp, D. J. The Innovation Gap in Pharmaceutical Drug Discovery & New Models for R & D Success https://www.semanticscholar.org/paper/The-Innovation-Gap-in-Pharmaceutical-Drug-Discovery-Hu-Schultz/b3b23901ff6b8f3726f819d9d6e7336f2a545244 (accessed 2021 -10 -11).

(12) Trost, B. M.; Fleming, I. *Comprehensive Organic Synthesis: Selectivity, Strategy, and Efficiency in Modern Organic Chemistry*, 1st ed.; Pergamon Press: Oxford, England New York, 1991.

(13) Pummangura, S.; Nichols, D. E.; McLaughlin, J. L. Cactus Alkaloids XXXIII: β-Phenethylamines from the Guatemalan Cactus Pilosocereus Maxonii. *Journal of Pharmaceutical Sciences* **1977**, *66* (10), 1485–1487. https://doi.org/10.1002/jps.2600661037.

(14) Katamura, T.; Shimizu, T.; Mutoh, Y.; Saito, S. Synthesis of Tricyclic Benzazocines by Aza-Prins Reaction. *Org. Lett.* **2017**, *19* (1), 266–269. https://doi.org/10.1021/acs.orglett.6b03577.

(15) Shi, F.; Cui, X. *Catalytic Amination for N-Alkyl Amine Synthesis*; Academic press: London, 2018.
(16) *Flammability Testing of Materials Used in Construction, Transport and Mining*; Apte, V. B., Ed.; Woodhead Publishing in materials; CRC Press: Boca Raton, Fla., 2006.
(17) Stock, N. L. Introducing Graduate Students to High-Resolution Mass Spectrometry (HRMS) Using a Hands-On Approach. *J. Chem. Educ.* **2017**, *94* (12), 1978–1982. https://doi.org/10.1021/acs.jchemed.7b00569.
(18) Zhu, R.; Jiang, J.-L.; Li, X.-L.; Deng, J.; Fu, Y. A Comprehensive Study on Metal Triflate-Promoted Hydrogenolysis of Lactones to Carboxylic Acids: From Synthetic and Mechanistic Perspectives. *ACS Catal.* **2017**, *7* (11), 7520–7528. https://doi.org/10.1021/acscatal.7b01569.

APPENDIX A: SUPPLEMENTAL INFORMATION

6,7-dimethoxy-1-phenethyl-2-tosyl-1,2,3,4-tetrahydroisoquinoline (#). KMB-1-011

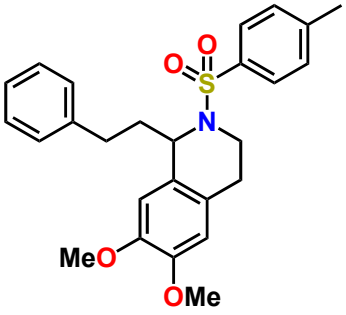

Yield: 97.6 mg, 90%; **Physical State:** white solid; **Melting Point:** 141-142°C; **TLC:** R_f = 0.58 (100% CH_2Cl_2, uv → PMA); **IR (thin film):** cm^{-1} 2999 (CH), 2938 (CH), 2849 (CH); **^{1}H NMR (CDCl$_3$, 400 MHz):** ***δ*** 7.60 (d, 2H, *J* = 8.0), 7.28 (t, 2H, *J* = 7.6 Hz), 7.20 (d, 1H. 1H, *J* = 9.3, 4.4), 3.92 (dt, 2H, *J* = 13.6 Hz, 3.2 Hz), 3.82 (s, 3H), 3.76 (s, 3H), 3.48 (m, 2H), 2.82 (m, 2H), 2.42 (m, 2H), 2.33 (s, 3H), 2.08 (m, 2H); **^{13}C {^{1}H} NMR (CDCl$_3$, 100MHz):** ***δ*** 147.8 (s), 147.5 (s), 143.0 (s), 141.8 (s), 138.0 (s), 129.4 (d), 128.5 (s), 128.5 (d), 128.4 (d), 127.0 (d), 125.9 (d), 124.6 (s), 111.3 (d), 109.5 (d), 56.2 (d), 56.0 (q), 55.8 (q), 39.2 (t), 38.8 (t), 38.8 (t), 32.9 (t), 25.7 (t), 21.4 (q); **HRMS (ESI):** Exact mass calcd for $C_{26}H_{29}NO_4S$ $[M+Na]^+$ *m/z* 474.170950. **Found** *m/z* 474.170453**.**

N-(3,4-dimethoxyphenethyl)-2-nitrobenzenesulfonamide (#). KMB-1-004 Yield: 1.81

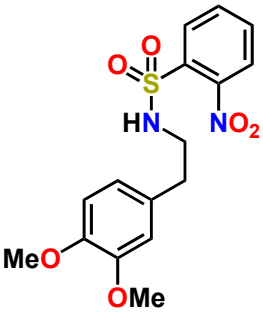

g, 90%; **Physical State:** tan solid; **Melting Point:** 112-115°C; **TLC:** R_f = 0.20 (1:1 Hexanes-Ethyl acetate, uv → PMA); **IR (thin film):** cm^{-1} 3225 (NH), 2939 (CH), 2836 (CH); **^{1}H NMR (400 MHz, CDCl$_3$):** 8.07-8.04 (m, 1H), 7.83-7.79 (m, 1H), 7.73-7.65 (m, 2H), 6.64 (dd, 1H, *J* = 8.4 Hz, 2.0 Hz), 6.71 (d, 1H, *J* = 8.4 Hz), 6.60 (d, 1H, *J* = 2.0 Hz), 5.39 (s, 1H), 3.83 (s, 3H), 3.80 (s, 3H), 3.38 (t, 2H, *J* = 6.8 Hz), 2.78 (t, 2H, *J* = 6.8 Hz); **^{13}C {^{1}H} NMR (100MHz, CDCl$_3$):** 149.0 (s), 147.9 (s), 147.8 (s), 133.8 (s), 133.4 (d), 132.8 (d), 130.8 (d), 129.9 (s), 125.3 (d), 120.8 (d), 111.7 (d), 111.4 (d), 55.9 (d), 55.8 (d), 45.2 (t), 35.6 (t); **HRMS (CI):** Exact mass calcd for $C_{18}H_{18}N_2O_6S$ $[M+Na]^+$ *m/z* 389.077411. **Found** *m/z* 389.077411.

N-(3,4-dimethoxyphenethyl)cyclopropanesulfonamide (#). KMB-1-009 Yield: 924.7

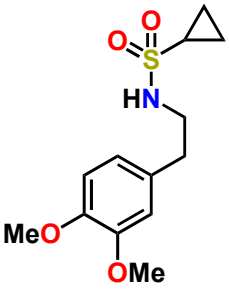

mg, 59%; **Physical State:** Clear oil; **TLC:** R_f = 0.4 (1:1 Hexanes-Ethyl acetate, uv → PMA); **IR (thin film):** cm^{-1} 3273 (NH), 2937 (CH), 2050 (C=C); **^{1}H NMR (400 MHz, CDCl$_3$):** ***δ*** 6.82 (d, 1H, *J* = 8.0 Hz), 6.77-6.73 (m, 2H), 4.25 (t, 1H, *J* = 6.0 Hz), 3.89 (s, 3H), 3.87 (s, 3H), 3.40 (q, 2H, *J* = 6.8 Hz), 2.83 (t, 2H, *J* = 6.8 Hz), 2.34 (tt, 1H, *J* = 12.8, 8.0, 4.8 Hz), 1.17-1.12 (m, 2H), 0.99-0.94 (m, 2H); **^{13}C {^{1}H} NMR (100MHz, CDCl$_3$):** ***δ*** 149.2 (s), 148.0 (s), 130.3 (s), 120.8 (d), 112.0 (d), 111.5 (d), 56.0 (q), 55.9 (q), 44.7 (t), 36.2 (t), 30.1 (d), 5.3 (t); **HRMS (CI):** Exact mass calcd for $C_{13}H_{19}NO_4S$ $[M+Na]^+$ *m/z* 308.092700. **Found** *m/z* 308.092663

N-(3,4-dimethoxyphenethyl)-2-methylpropane-2-sulfinamide (#). DPC-1-014 Yield:

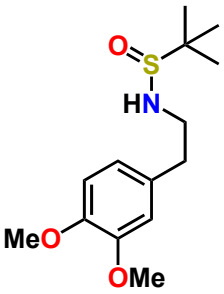

1.00 g, 57%; **Physical State:** white solid; **Melting Point:** 93-96°C; **TLC:** R_f = 0.50 (4:1 Hexanes-Ethyl acetate, uv → PMA); **IR (thin film):** cm^{-1} 3217 (NH), 2917 (CH), 2856 (CH); **^{1}H NMR (400 MHz, $CDCl_3$):** 6.81 (d, 1H, *J* = 8.6 Hz), 6.76 (d, 1H, *J* = 1.8 Hz), 6.74 (d, 1H, *J* = 1.8 Hz), 3.87 (s, 3H), 3.87 (s, 3H), 3.44 (ddd, 1H, *J* = 19.5, 12.8, 6.7 Hz), 3.32 (ddd, 1H, *J* = 13.8, 6.7 Hz), 3.22 (t, 1H, *J* = 6.2 Hz), 2.84 (dp, 2H, *J* = 13.8, 6.7 Hz), 1.18 (s, 9H); **^{13}C {^{1}H} NMR (100MHz, $CDCl_3$):** 149.0 (s), 147.7 (s), 131.1 (s), 120.9 (d), 112.2 (d), 111.3 (d), 55.9 (q), 55.9 (q), 55.7 (s), 47.2 (t), 47.2 (t), 37.1 (t), 22.6 (q); **HRMS (CI):** Exact mass calcd for $C_{14}H_{23}NO_3S$ $[M+Na]^+$ *m/z* 308.129085. **Found** *m/z* 308.128800.

N-(3,4-dimethoxyphenethyl)-2-methylpropane-2-sulfonamide (#). DPC-1-015 Yield:

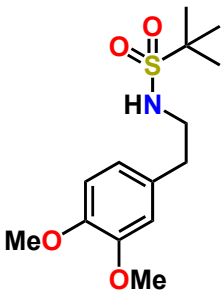

926 mg, 88%; **Physical State:** white solid; **Melting Point:** 106-108°C; **TLC:** R_f = 0.51 **^{1}H NMR (400 MHz, $CDCl_3$):** 6.82 (s, 1H), 6.77 (d, 1H, *J* = 8.0 Hz), 6.74 (d, 1H, *J* = 8.0), 3.88 (s, 3H), 3.82 (s, 3H), 3.57 (t, 1H, *J* = 6.0 Hz), 3.41 (q, 2H, *J* = 6.7 Hz), 2.83 (t, 2H, *J* = 7.7 Hz), 1.36 (s, 9H); **^{13}C {^{1}H} NMR (100MHz, $CDCl_3$):** 149.2 (s), 147.9 (s), 130.4 (s), 120.9 (d), 112.1 (d), 111.5 (d), 59.9 (s), 56.0 (q), 55.9 (q), 46.2 (t), 37.2 (t), 24.3 (q); **HRMS (CI):** Exact mass calcd for $C_{14}H_{23}NO_4S$ $[M+Na]^+$ *m/z* 324.124000. **Found** *m/z* 324.123812

2-(cyclopropylsulfonyl)6,7-dimethoxy-1-phenethyl-1,2,3,4-tetrahydroisoquinoline

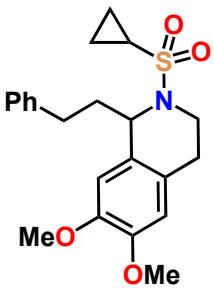

(#). GJR-5-024 Yield: 101.3 mg, 89%; **Physical State:** clear oil; **TLC:** R_f = 0.6 (100% dichloromethane, uv → PMA); **IR (thin film):** cm^{-1} 3000 (CH), 2936 (CH); **^{1}H NMR ($CDCl_3$, 400 MHz): *δ*** 7.30-7.23 (m, 4H), 7.19-7.16 (m, 1H), 6.58 (s, 1H), 6.42 (s, 1H), 4.78 (dd, 1H, *J* = 10.0, 4.0 Hz), 4.01 (dd, 1H, *J* = 15.2, 4.0 Hz), 3.84 (s, 3H), 3.82 (s, 3H), 3.51 (ddd, 1H, *J* = 17.2, 12.0, 5.2 Hz), 3.07 (ddd, 1H, *J* = 16.8, 12.0, 6.8), 2.91-2.79 (m, 2H), 2.68 (dd, 1H, *J* = 16.8, 4.0 Hz), 2.20-1.98 (m, 3H), 1.19-1.17 (m, 1H), 1.10-1.06 (m, 1H), 0.85-0.81 (m, 1H), 0.75-0.71 (m, 1H); **^{13}C {^{1}H} NMR ($CDCl_3$, 100MHz): *δ*** 148.0 (s), 147.7 (s), 141.8 (s), 129.1 (d), 128.5 (d), 128.4 (d), 125.9 (s), 124.5 (s), 111.6 (d), 109.5 (d), 56.1 (d), 56.0 (q), 55.9 (q), 38.9 (t), 38.5 (t), 32.9 (t), 30.2 (d), 26.7 (t), 5.7 (t), 5.4 (t); **HRMS (ESI):** Exact mass calcd for $C_{22}H_{27}NO_4S$ $[M+Na]^+$ *m/z* 424.155300. **Found** *m/z* 424.155336.

2-(mesitylsulfonyl)-6,7-dimethoxy-1-phenethyl-1,2,3,4-tetrahydroisoquinoline (#). GJR-5-009 Yield: 55.8 mg, 49%; **Physical State:** clear oil; **TLC:** R_f = 0.48 (100% Dichloromethane, uv → PMA); **IR (thin film):** cm^{-1} 2937 (CH), 1735 (C=C); **^{1}H NMR ($CDCl_3$, 400 MHz): *δ*** 7.23 (td, 2H, *J* = 7.6, 1.2 Hz), 7.15 (tt, 1H, *J* = 7.6, 1.2 Hz), 7.03 (dd, 2H, *J* = 4.4, 1.2 Hz), 6.95 (s, 2H), 6.53 (s, 1H), 6.46 (s, 1H), 4.66 (q, 1H, *J* = 4.4 Hz), 3.89 (dd, 1H, *J* = 9.2, 6.0 Hz), 3.82 (s, 3H), 3.81 (s, 3H), 3.44 (ddd, 1H, *J* = 14.0, 12.0, 4.4 Hz), 2.81 (ddd, 1H, *J* = 16.4, 12.0, 6.4 Hz), 2.62 (ddd, 1H, *J* = 14.0, 10.8, 5.2), 2.59 (s, 6H), 2.58-2.50 (m, 1H), 2.37-2.32 (m, 1H), 2.30 (s, 3H), 2.10 (m, 1H), 1.99 (m, 1H); **^{13}C {^{1}H} NMR ($CDCl_3$, 100MHz): *δ*** 147.9 (s), 147.8 (s), 142.4 (s), 141.6 (s), 140.2 (s), 133.6 (s), 132.0 (d), 128.9 (s), 128.4 (d), 128.3 (d), 125.9 (d), 125.2 (s), 111.7 (d), 109.6 (d), 56.0 (d), 55.8 (q), 55.7 (q), 38.9 (t), 38.2 (t), 32.6 (t), 27.2 (t), 23.0 (q), 21.1 (s); **HRMS (ESI):** Exact mass calcd for $C_{28}H_{33}NO_4S$ $[M+Na]^+$ *m/z* 502.202250. **Found** *m/z* 502.201585.

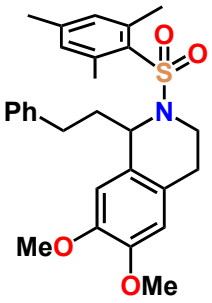

1-ethyl-6,7-dimethoxy-2-tosyl-1,2,3,4-tetrahydroisoquinoline (#). DPC-1-030 Yield: 108.2 mg, 97%; **Physical State:** clear oil; **TLC:** R_f = 0.29 (2:1 Hexanes-Ethyl acetate, uv → PMA); **IR (thin film):** cm^{-1} 2965 (CH), 2933 (CH); **^{1}H NMR ($CDCl_3$, 400 MHz): *δ*** 7.59 (d, 2H, *J* = 8.0 Hz), 7.11 (d, 2H, *J* = 8.0 Hz), 6.53 (s, 1H), 6.34 (s, 1H), 4.81 (dd, 1H, *J* = 8.4, 6.4 Hz), 3.86 (s, 3H), 3.85 (m, 1H), 3.77 (s, 3H), 3.40 (ddd, 1H, *J* = 14.4, 9.6, 6.8 Hz), 2.41 (m, 2H), 2.33 (s, 3H), 1.79 (m, 2H), 1.79 (m, 2H), 1.04 (t, 3H, *J* = 7.6 Hz); **^{13}C {^{1}H} NMR ($CDCl_3$, 100MHz): *δ*** 148.0 (s), 147.7 (s), 141.8 (s), 129.1 (d), 128.5 (d), 128.4 (d), 125.9 (s), 124.5 (s), 111.6 (d), 109.5 (d), 56.1 (d), 56.0 (q), 55.9 (q), 38.9 (t), 38.5 (t), 32.9 (t), 30.2 (d), 26.7 (t), 5.7 (t), 5.4 (t); **HRMS (ESI):** Exact mass calcd for $C_{20}H_{25}NO_4S$ $[M+Na]^+$ *m/z* 398.139650. **Found** *m/z* 398.139658**.**

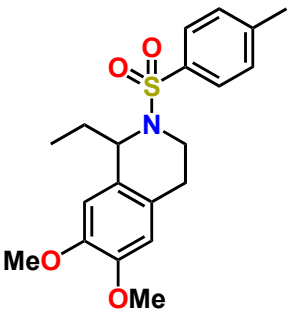

1-butyl-6,7-dimethoxy-2-tosyl-1,2,3,4-tetrahydroisoquinoline (#). EBC-4-042 Yield: 10.6 mg, 22%; **Physical State:** clear oil; **TLC:** R_f = 0.75 (9:1 Dichloromethane-Ethyl acetate, uv → PAA); **IR (thin film):** cm^{-1} 2921 (CH), 2361 (C-H); **^{1}H NMR ($CDCl_3$, 400 MHz): *δ*** 7.58 (d, 2H, *J* = 8.0 Hz), 7.11 (d, 2H, *J* = 8.0 Hz), 6.51 (s, 1H), 6.33 (s, 1H), 4.87 (dd, 1H, *J* = 9.5, 4.8 Hz), 3.87 (m, 1H), 3.86 (s, 3H), 3.77 (s, 3H), 3.42 (ddd, 1H, *J* = 14.5, 9.8, 6.8 Hz), 2.41 (dd, 2H, *J* = 6.5, 3.5 Hz), 2.33 (s, 3H), 1.73 (m, 2H), 1.40-1.34 (m, 4H), 0.90 (t, 3H, *J* = 7.2 Hz); **^{13}C {^{1}H} NMR ($CDCl_3$, 100MHz): *δ*** 147.7 (s), 147.4 (s), 142.9 (s), 138.1 (s), 129.3 (d), 129.1 (s), 127.0 (d), 124.6 (s), 111.3 (d), 109.6 (d), 56.4 (d), 56.0 (q), 55.8 (s), 38.5 (t), 37.3 (t), 28.7 (t), 25.7 (t), 22.5 (t), 21.4 (q), 14.0 (q); **HRMS (ESI):** Exact mass calcd for $C_{22}H_{29}NO_4S$ $[M]^+$ *m/z* 426.17950. **Found** *m/z* 426.170556**.**

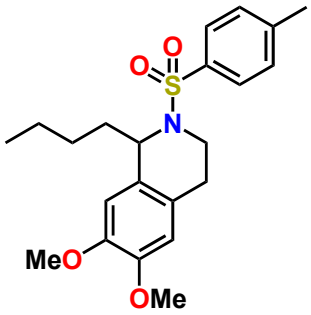

1-pentyl-6,7-dimethoxy-2-tosyl-1,2,3,4-tetrahydroisoquinoline (#). DPC-1-027 Yield:

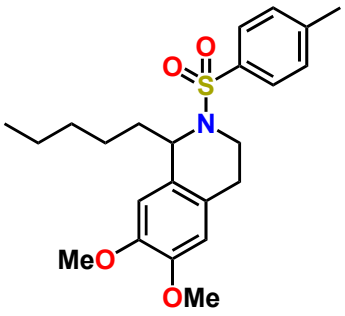

132.3 mg, quant.; **Physical State:** clear oil.; **TLC:** R_f = 0.42 (100% dichloromethane, uv → PMA); **IR (thin film):** cm^{-1} 2925 (CH), 2854 (CH); **^{1}H NMR ($CDCl_3$, 400 MHz): δ** 7.58 (d, 2H, *J* = 8.0 Hz), 7.10 (d, 2H, *J* = 8.0 Hz), 6.51 (s, 1H), 6.33 (s, 1H), 4.87 (dd, 1H, *J* = 8.8, 4.8 Hz), 3.89 (ddd, 1H, *J* = 4.8, 2.4, 1.6 Hz), 3.86 (s, 3H), 3.77 (s, 3H), 3.41 (ddd, 1H, *J* = 14.8, 10.4, 6.4 Hz), 2.45-2.39 (m, 2H), 2.32 (s, 3H), 1.71 (m, 2H), 1.49-1.41 (m, 2H), 1.36-1.27 (m, 4H), 0.88 (t, 3H, *J* = 7.2 Hz); **^{13}C {^{1}H} NMR ($CDCl_3$, 100MHz): δ** 147.7 (s), 147.3 (s), 142.9 (s), 138.1 (s), 129.3 (d), 129.1 (s), 127.0 (d), 124.6 (s), 111.3 (d), 109.6 (d), 56.4 (d), 56.0 (q), 55.8 (q), 38.5 (t), 37.5 (t), 31.6 (t), 26.2(t), 25.8 (t), 22.6 (t), 21.4 (q), 14.1 (q); **HRMS (CI):** Exact mass calcd for $C_{23}H_{31}NO_4S$ $[H]^+$ *m/z* 418.204656. **Found** *m/z* 418.204840.

1-cyclohexyl-6,7-dimethoxy-2-tosyl-1,2,3,4-tetrahydroisoquinoline (#). KMB-1-043

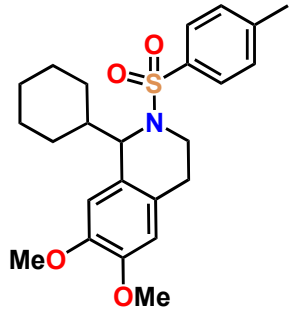

Yield: 97.6 mg, 95%; **Physical State:** clear oil; **TLC:** R_f = 0.40 (100% dichloromethane, uv → PMA); **IR (thin film):** cm^{-1} 3272 (NH), 2938 (CH); **^{1}H NMR ($CDCl_3$, 400 MHz): δ** 7.47 (d, 2H, *J* = 8.0 Hz), 7.03 (d, 2H, *J* = 8.0 Hz), 6.48 (s, 1H), 6.30 (s, 1H), 4.51 (d, 1H, *J* = 8.8 Hz), 3.85 (s, 3H), 3.75 (s, 3H), 3.72 (ddd, 1H, *J* = 13.5, 7.2, 6.8 Hz), 3.54 (ddd, 1H, *J* = 14.4, 9.2, 5.6 Hz), 2.54 (ddd, 1H, *J* = 16.4, 6.0, 4.4 Hz), 2.38 (ddd, 1H, 16.4, 8.0, 4.4 Hz), 2.29 (s, 3H), 2.10-2.00 (m, 2H), 1.81-1.60 (m, 5H), 1.71-1.10 (m, 2H); **^{13}C {^{1}H} NMR ($CDCl_3$, 100MHz): δ** 147.8 (s), 145.5 (s), 142.7 (s), 137.4 (s), 129.0 (d), 127.4 (s), 127.3 (d), 125.1 (s), 111.5 (d), 111.3 (d), 61.8 (d), 56.1 (q), 55.8 (q), 42.9 (d), 39.6 (t), 30.7 (t), 30.4 (t), 26.3 (t), 26.2 (t), 25.3 (t), 21.4 (q); **HRMS (ESI):** Exact mass calcd for $C_{24}H_{31}NO_4S$ $[M+Na]^+$ *m/z* 452.186600. **Found** *m/z* 452.186723**.**

1-(benzyloxy)methyl)-6,7-dimethoxy-2-tosyl-1,2,3,4-tetrahydroisoquinoline (#).

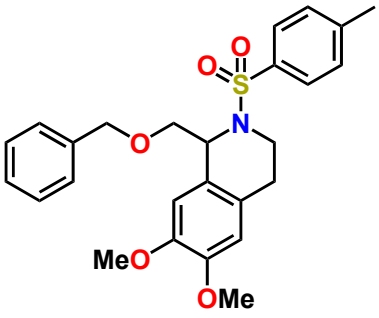

GJR-5-023 Yield: 98.5 mg, 88%; **Physical State:** clear oil; **TLC:** R_f = 0.68 (100% dichloromethane, uv → PMA); **IR (thin film):** cm^{-1} 2935 (CH), 2861 (CH); **^{1}H NMR ($CDCl_3$, 400 MHz): δ** 7.69 (d, 2H, *J* = 8.4 Hz), 7.34-7.20 (m, 5H), 7.14 (d, 2H, *J* = 8.4 Hz), 6.61 (s, 1H), 6.46 (s, 1H), 5.13 (t, 1H, *J* = 3.2 Hz), 4.53 (d, 1H, *J* = 12.0 Hz), 4.44 (d, 1H, *J* = 12.0 Hz), 3.82-3.77 (m, 2H), 3.79 (s, 3H), 3.77 (s, 3H), 3.66 (dd, 1H, *J* = 9.6, 3.2 Hz), 3.48 (ddd, 1H, *J* = 14.0, 11.2, 4.8 Hz), 2.71-2.50 (m, 1H), 2.50 (dt, 1H, *J* = 12.0, 4.0 Hz); **^{13}C {^{1}H} NMR ($CDCl_3$, 100MHz): δ** 148.0 (s), 147.3 (s), 143.1 (s), 138.0 (s), 137.8 (s), 129.4 (d), 128.3 (d), 127.6 (d), 127.6 (d), 127.2 (d), 126.1 (s), 125.2 (s), 111.3 (d), 110.2 (d), 73.7 (t), 73.0 (t), 55.9 (q), 55.8 (q), 55.2 (d), 40.1 (t), 27.0 (t); **HRMS (CI):** Exact mass calcd for $C_{26}H_{29}NO_5S$ $[M+Na]^+$ *m/z* 490.165865. **Found** *m/z* 490.166085

1-cyclopropyl-6,7-dimethoxy-2-tosyl-1,2,3,4-tetrahydroisoquinoline (#). DPC-1-028

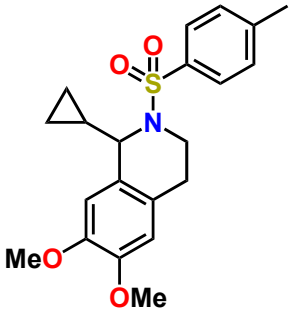

Yield: 67 mg, 58%; **Physical State:** clear oil; **TLC:** R_f = 0.40 (100% dichloromethane, uv → PMA); **IR (thin film):** cm^{-1} 3003 (CH), 2934 (CH), 2835 (CH); **^{1}H NMR ($CDCl_3$, 400 MHz): *δ*** 7.59 (d, 2H, *J* = 7.6 Hz), 7.13 (d, 2H, *J* = 7.6 Hz), 6.63 (s, 1H), 6.38 (s, 1H), 4.37 (d, 1H, *J* = 8.0 Hz), 3.90 (m, 1H), 3.86 (s, 3H), 3.79 (s, 3H), 3.61 (ddd, 1H, *J* = 16.8, 10.4, 6.4 Hz), 2.50 (m, 2H), 2.34 (s, 3H), 1.21 (m, 1H), 0.68 (m, 1H), 0.56 (m, 3H); **^{13}C {^{1}H} NMR ($CDCl_3$, 100MHz): *δ*** 148.0 (s), 147.2 (s), 142.9 (s), 138.2 (s), 129.3 (d), 127.9 (s), 127.0 (d), 125.0 (s), 111.3 (d), 110.0 (d), 60.0 (d), 56.0 (q), 55.8 (q), 39.4 (t), 26.3 (t), 21.4 (q), 18.3 (d), 5.6 (t), 3.5 (t); **HRMS (ESI):** Exact mass calcd for $C_{21}H_{25}NO_4S$ $[M+Na]^+$ *m/z* 410.139650. **Found** *m/z* 410.138845.

Ethyl-6,7-dimethoxy-2-tosyl-1,2,3,4-tetrahydroisoquinoline-1-carboxylate (#). GJR-4-008

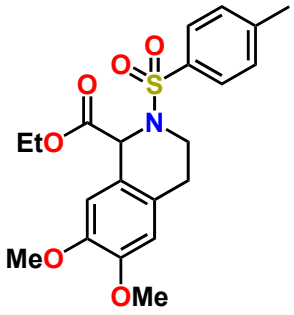

Yield: 26.3 mg, 26%; **Physical State:** clear oil; **TLC:** R_f = 0.4 (100% CH_2Cl_2, uv → PMA); **IR (thin film):** cm^{-1} 2936 (CH), 2255 (C=C), 1735 (C=O); **^{1}H NMR ($CDCl_3$, 400 MHz): *δ*** 7.71 (d, 2H, *J* = 8.0 Hz), 7.27 (d, 2H, *J* = 8.0 Hz), 6.90 (s, 1H), 6.55 (s, 1H), 5.45 (s, 1H), 4.02 (dq, 2H, *J* = 14.4, 7.2, 1.6 Hz), 3.84 (s, 3H), 3.83 (s, 3H), 3.80 (ddd, 2H, *J* = 16.0, 10.0, 6.4 Hz), 2.81 (dt, 2H, *J* = 16.0, 5.6 Hz), 2.41 (s, 3H), 1.17 (t, 3H, *J* = 8.0 Hz); **^{13}C {^{1}H} NMR ($CDCl_3$, 100MHz): *δ*** 170.5 (s), 148.7 (s), 147.7 (s), 143.5 (s), 136.7 (s), 129.6 (d), 127.2 (d), 126.3 (s), 121.5 (s), 111.4 (d), 109.9 (d), 61.5 (t), 57.4 (d), 56.0 (q), 55.9 (q), 40.8 (t), 27.9 (t), 21.5 (q), 14.0 (q); **HRMS (ESI):** Exact mass calcd for $C_{21}H_{25}NO_6S$ $[M]^+$ *m/z* 420.147535. **Found** *m/z* 420.146935.